Acta Geologica Sinica (English Edition), 2019, 93(5): 1300–1316

Early Permian A-type Granites in the Zhangdaqi Area, Inner Mongolia, China and Their Tectonic Implications

ZHANG Li[1, 2], LIU Yongjiang[3, 4, *], SHAO Jun[2], LI Weimin[1], LIANG Chenyue[1], CHANG Ruihong[1], YANG Hongzhi[2], FENG Zhiqiang[5], ZHANG Chao[2], XU Jia[2], SHI Yi[2], YANG Fan[2] and HE Pengfei[2]

[1] *College of Earth Sciences, Jilin University, Changchun 130061, China*
[2] *Shenyang Institute of Geology and Mineral Resources, China Geological Survey, Shenyang 110034, China*
[3] *Key Lab of Submarine Geoscience and Prospecting Techniques, MOE, Institute for Advanced Ocean Study, College of Marine Geosciences, Ocean University of China, Qingdao 266100, China*
[4] *Laboratory for Marine Mineral Resources, Qingdao National Laboratory for Marine Science and Technology, Qingdao 266100, China*
[5] *College of Mining Engineering, Taiyuan University of Technology, Taiyuan 030024, China*

Abstract: There is a controversy regarding the amalgamation of Xing'an and Songnen Blocks along the Hegenshan-Heihe Suture (HHS) in the eastern Central Asian Orogenic Belt (CAOB). To solve this problem, we performed detailed study on the granites from the Zhangdaqi area, adjacent to the north of the HHS in the northern part of the Great Xing'an Range, NE China. Geochemically, the granites in the study area are metaluminous-weak peraluminous and high-K calc-alkaline series. Trace elements of the granites show that LREEs are relatively enriched, while HREEs are relatively deficient and obvious REE fractionation. The granites are characterized by obvious negative Eu anomalies, meanwhile, they are relatively enriched in Rb, K, Th and depleted in Ba, Nb, Sr, P, Ti. All the geochemical features suggest that the granites in the Zhangdaqi area are aluminum A-type granites. The zircon LA-ICP-MS U-Pb ages of these granites are 294–298 Ma, indicating that they formed in the Early Permian. These granites also have positive $\varepsilon_{Hf}(t)$ values (8.4–14.2) and a relatively young two-stage model age between 449 Ma and 977 Ma, implying that the magma was derived from the re-melting of the Early Paleozoic-Neoproterozoic juvenile crust. Combined with geochemical characteristics (Nb/Ta ratios of 9.0–22.2, and Zr/Hf ratios of 52.3–152.0), we believe that the magmatic source area is a mixture of partial melting of the lower crust and depleted mantle. A-type granites and bimodal volcanic rocks along the Hegenshan-Heihe Suture formed during the Late Carboniferous-Early Permian, indicating that the HHS between Xing'an and Songnen Blocks closed in the late Early-Carboniferous. Subsequently, the Zhangdaqi area was in a post-orogenic extensional environment from Late Carboniferous to Early Permian and resulted in the formation of the A-type granites.

Key words: Central Asian Orogenic Belt, Hegenshan-Heihe Suture, A-type granites, zircon U-Pb age, Lu-Hf isotopic, NE China

Citation: Zhang et al., 2019. Early Permian A-type Granites in the Zhangdaqi Area, Inner Mongolia, China and Their Tectonic Implications. Acta Geologica Sinica (English Edition), 93(5): 1300–1316. DOI: 10.1111/1755-6724.14385

1 Introduction

The Central Asian Orogenic Belt (CAOB) is a huge accretionary orogenic belt, and it attracted many scholars' attention due to the special geological development history (Hong et al., 2000, 2004; Wu et al., 2000; Wang et al., 2009; Xiao et al., 2009a, 2014, 2015; Xia et al., 2012; Ma et al., 2015; Tang et al., 2015). Northeast China (NE China) is the eastern part of the CAOB which mainly consists of Erguna Block, Xing'an Block, Songnen Block, Jiamusi-Brea Block and the accretionary belts of continental margin, as well as the main suture zones between these blocks (Figs. 1a, 1b) (Zhang et al., 2006; Xu et al., 2014; Liu et al., 2010, 2017). During the evolution of the Paleo-Asian Ocean, a complex collage process occurred among the blocks (Xiao et al., 2009b; Liu et al., 2017, 2019).

The Hegenshan-Heihe Suture (HHS) records the amalgamation of Xing'an and Songnen Blocks (Sun et al, 2001; Wu et al., 2002; Liu et al., 2017). It is one of the most important and regional sutures between Siberia Plate and North China Plate. However, the amalgamation is still controversial because of the lack of ophiolite in the northern part of HHS. The emplacement of A-type granites generally represents the end of orogeny (Zhang et al., 2003). In recent years, some relevant studies were performed on A-type granites on northern sides of the suture, providing a basis for the combination time of Xing'an and Songnen Blocks (Wu et al., 2002; Shi et al., 2004; Liu, 2009; Zhang et al., 2009; Sui et al., 2009; Han et al., 2010; Tong et al., 2010, 2015; Guo et al., 2011; Qu

* Corresponding author. E-mail: liuyongjiang@ouc.edu.cn

© 2019 Geological Society of China

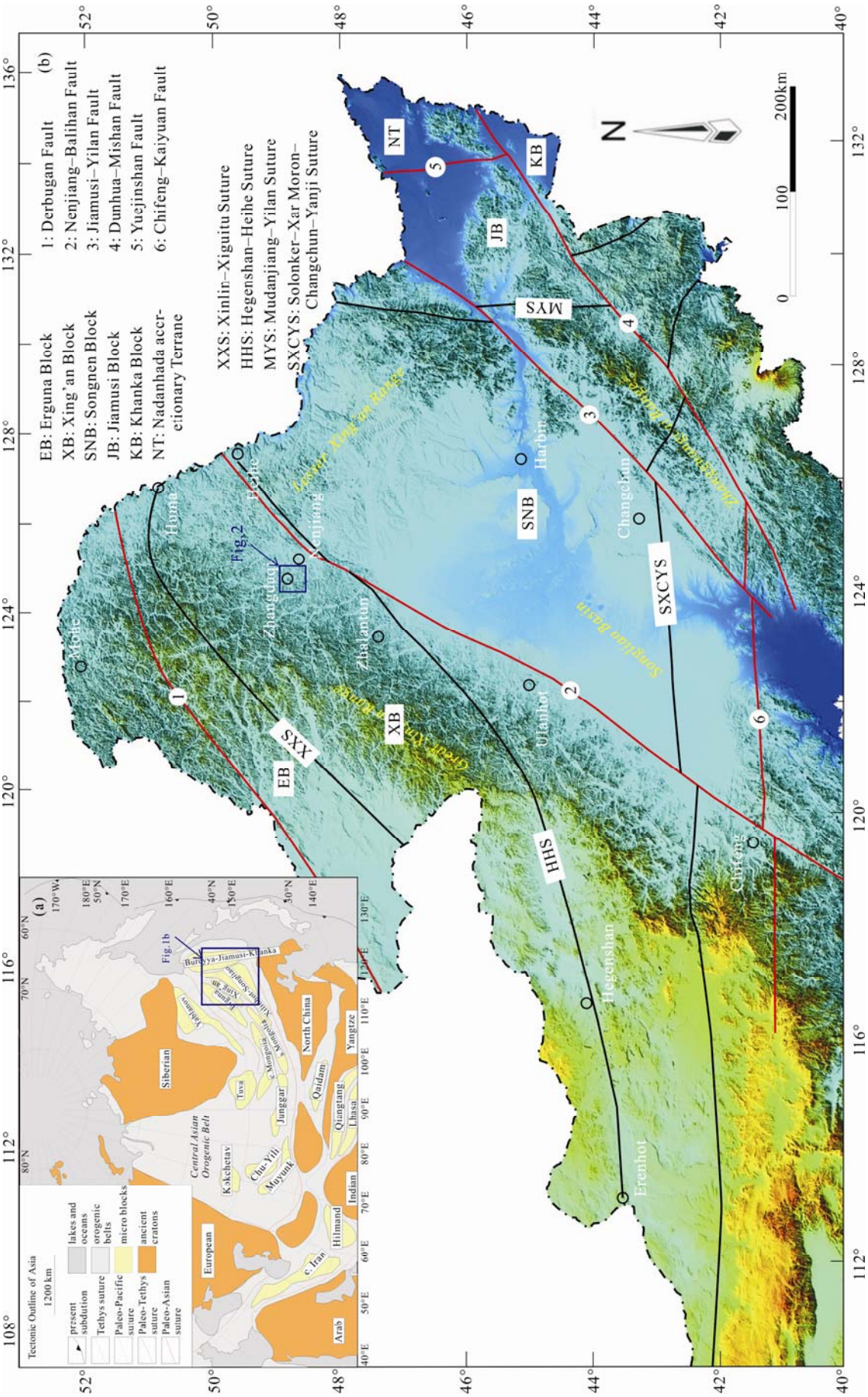


Fig. 1. (a) Tectonic online of Asia; (b) tectonic division of NE China (after Liu et al., 2017).

et al., 2011; Zhang et al., 2011; Cheng et al., 2012; Zhao et al., 2013; Shao et al., 2014; Zhang et al., 2016; Kong et al., 2017; Yang et al., 2017; Wang et al., 2017; Shi et al., 2019). Nevertheless, there are still some problems as follows: (1) Is the crystallization age of A-type granites Late Carboniferous (Qu et al., 2011; Zhang et al., 2011; Cheng et al., 2012; Zhao et al., 2013; Kong et al., 2017; Yang et al., 2017; Wang et al., 2017; Shi et al., 2019) or Early Permian (Wu et al., 2002; Sui et al., 2009; Liu, 2009; Zhang et al., 2009; Guo et al., 2011)? (2) Is the detail type of the granites Non-orogenic A1-type granite (Shi et al., 2004; Zhang et al., 2009; Tong et al., 2015; Zhang et al., 2016) or Post-orogenic A2-type granite (Shao et al., 2014; Tong et al., 2015; Zhang et al., 2016)? (3) Is the magma from partially molten material in the lower crust (Guo et al., 2011) or from a mixture of crust and mantle (Wu et al., 2002; Han et al., 2010)? (4) Is the tectonic setting subduction and subsequent collision (Hong et al., 1991) or the extension after collision (Shi et al., 2004; Zhang et al., 2009; Guo et al., 2011)? To answer these questions, we performed geochemistry and geochronology analysis on A-type granites exposed in the zhangdaqi area, to determine their crystallization age, petrogenesis, and tectonic setting. This research provides the constraint on the amalgamation of Xing'an and Songnen Blocks.

2 Geological Setting

The Zhangdaqi area is located in the eastern part of the Northern Greater Xing'an Range adjacent to the north side of Hegenshan-Heihe suture (Fig. 1). Multiple Late Paleozoic granite outcrops exist in this area (Fig. 2). According to the recent research of the Zhangdaqi Regional Geological Survey Project, these granites can be divided into Middle Devonian-Early Carboniferous granodiorite and monzogranite, Early Permian granodiorite, monzogranite and alkali feldspar granite, Early Cretaceous monzogranite and diorite. In addition, the outcrop strata contain three groups, including Neoproterozoic Xinghuadukou Group, Late Silurian Woduhe group and Early Cretaceous volcanic rocks. The Xinghuadukou Group is primarily composed of plagioclase hornblende gneiss, while the Woduhe Group is sporadically distributed in the Late Paleozoic granites and consists of argillaceous slate, metasandstone and silty metamorphic. The Early Cretaceous volcanic rocks mainly distributed in the south of study area (Fig. 2). In this study, we focus on the Early Permian monzogranite and alkali feldspar granite.

3 Samples Collection and Analytical Methods

3.1 Samples collection

We collected four samples from research area in the Zhangdaqi (16TK19TW1: 124°08′08″E, 49°19′12″N, 16TK22TW1: 124°15′56″E, 49°23′00″N, 16TK28TW1: 124°18′10″E, 49°24′39″N, 16TK29TW1: 124°16′24″E, 49°24′22″N). Detail sample locations are shown in Fig. 2. Petrographically described as follow.

Sample 16TK19TW1 and 16TK28TW1 are monzogranite that collected from Dongfengshou and Yilijiudui. The sample exhibits a classical granitic texture and the size of the mineral grain range from medium to fine. The mineral assemblage presented are plagioclase (~30%) with grain size of 0.4–2.5 mm, alkali feldspar (~35%) with grain size of 1–3 mm, quartz (~30%) with grain size of 0.3–2 mm, biotite (<5%) with grain size of 0.5 mm (Figs. 3a, 3b, 3d, 3e) and some accessory minerals consisting of magnetite, zircon, apatite and titanite.

Sample 16TK22TW1 and 16TK29TW1 are alkali-feldspar granite that collected from Yilijiudui. The size of the mineral grain ranges from fine to medium with granitic texture. The granites consist mainly quartz (~40%) with the grain size of 1–5 mm, alkali feldspar most of perthite (~60%) with the grain size of 1–4 mm (Figs. 3c, 3f), and the accessory minerals consisting of magnetite, zircon and ilmenite.

3.2 Analytical methods

The analyses of major and trace elements were completed in the Northeast Mineral Resources and Supervision Testing Center, Ministry of Land and Resources, Shenyang, China. The analyzing samples were unweathered rocks, and the analytical process was carried out in pollution-free equipment. Major elements concentrations were determined by X-ray fluorescence spectrometry (XRF), the analytical precision is better than 5%. Trace elements were determined by ICP-MS, the analytical precision is better than 8%.

Separation of zircon grains was completed at Institute of Regional Geology and Mineral Survey Laboratory, Hebei Province, China. Targetry and photography of zircon grains were completed at Beijing Zhongxingmeike Technology co. LTD, Beijing, China. Zircon LA-ICP-MS U-Pb dating and Lu-Hf isotope analysis were completed at Isotopic Laboratory, Tianjin Institute of Geology and Mineral Resources, Tianjin, China. After crushing, washing, magnetic separation and heavy liquid separation, zircon grains were selected by binoculars with purity over 99%, then the zircon grains were fixed with epoxy resin and polished to expose the core. Before analyzing，the zircon surface was cleaned by 3% nitric acid solution, in order to remove surface stains, translucent, reflective and cathode-luminescence (CL) photography were then performed.

During zircon U-Pb dating, Laser Denudation System (LA) was NEWWave 193 mm FX ARF, which was made in the ESI Company (USA). MC-ICP-MS (Multireceiver Inductively Coupled Plasma Mass Spectrometer) was Neptune, which was made in the Thermo Fisher Company (USA). The laser denudation process used helium as carrier and argon as auxiliary gas to adjust sensitivity. 350 groups of data were collected at every denudation point, and ICPMSDataCal was adopted for offline processing of collected data (Liu et al., 2008). The laser beam had a diameter of 35 μm and a frequency of 8Hz. Isotope fractionation correction used zircon standard GJ-1 as external standard, U-Th-Pb isotopic ratio and U, Pb content of zircon standard GJ-1 were quote from Elhlou et al. (2006). Concord diagrams drawing and weighted average calculation of zircon used Isoplot/Ex_ver3

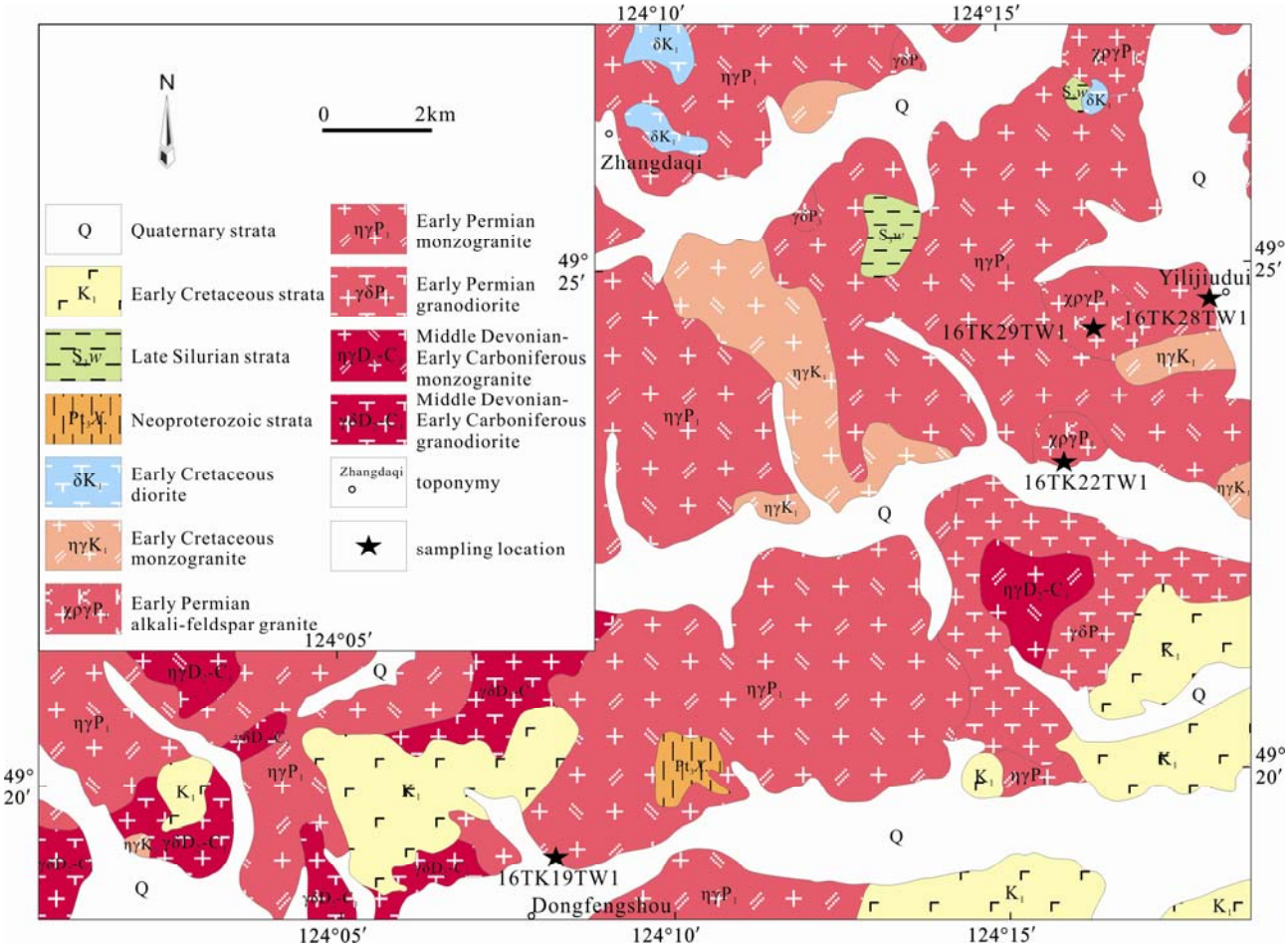


Fig. 2. Geological map of the Zhangdaqi area (see Fig. 1b for location).

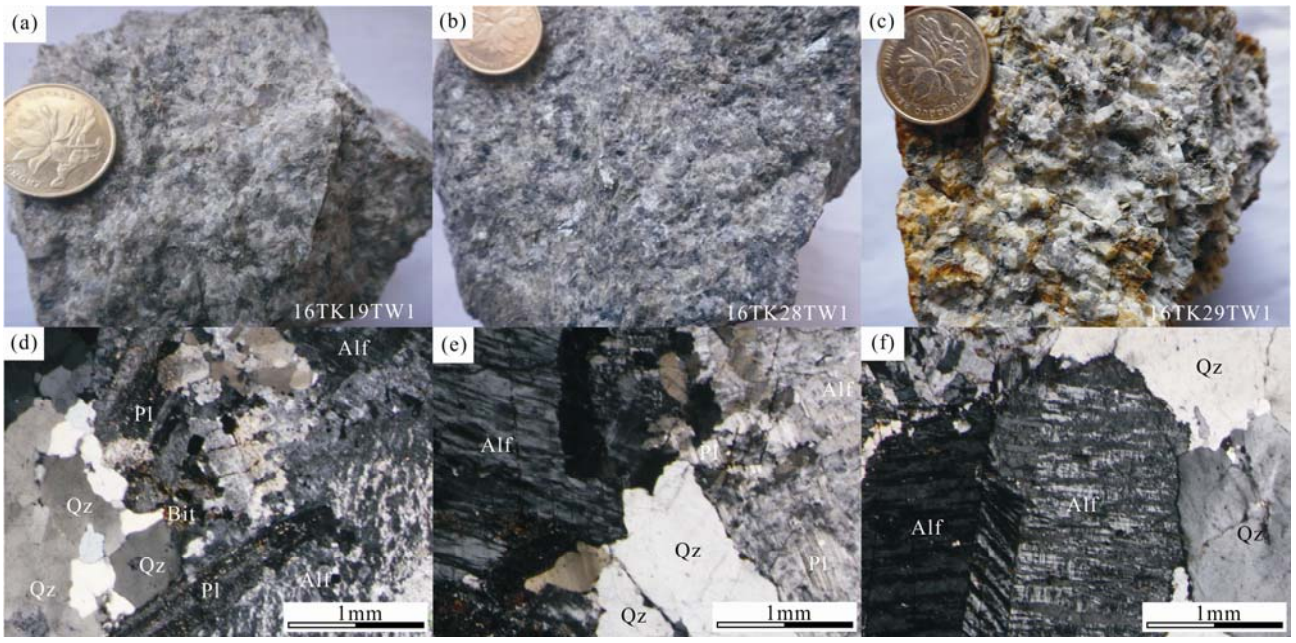


Fig. 3. Hand specimens and micrographs of monzogranite and alkali-feldspar granite in the Zhangdaqi area.
Q-Quartz, Af-Alkali Feldspar, Pl-Plagioclase, Bi-Biotite.

(Ludwig, 2003).

Zircon Lu-Hf isotopic assay used Neptune system, and analytical point was at or near the same location of zircon U-Pb dating, analysis conditions, instrument model and technological process referring to Geng et al. (2011). The $\varepsilon_{Hf}(t)$ value was calculated based on the $^{206}Pb/^{238}U$ age of zircon. Decay constant of ^{176}Lu is 1.867×10^{-11}/y (Amelin and Davis, 2005), $^{176}Hf/^{177}Hf$ ratios and $^{176}Lu/^{177}Hf$ ratios of chondrite is 0.282785 and 0.0336 (Bouvier et al., 2008). The model age of depleted mantle was calculated based on $^{176}Hf/^{177}Hf$ ratios (0.283250) and $^{176}Lu/^{177}Hf$ ratios (0.0384) (Griffin et al., 2000), the crust model age of zircon Hf isotopic was calculated based on $^{176}Lu/^{177}Hf$ ratios (0.015) (Griffin et al., 2002).

4 Results

4.1 Geochemistry

Major (wt%) and trace (ppm) elements data for the granites in the Zhangdaqi area are showing in Table 1.

The samples (16TK19TW1, 16TK22TW1, 16TK29TW1) contain high concentrations of SiO_2 (73.47–77.54 wt%, average of 75.35 wt%), Al_2O_3 (11.36–13.59 wt%, average of 12.34 wt%) and (Na_2O+K_2O) (9.00–9.38 wt%, average of 9.18 wt%), the ratio of K_2O to Na_2O is 0.95–1.63 with the average of 1.37. Meanwhile, it contains relatively low concentrations of CaO (0.01–0.53 wt%), MgO (0.05–0.54 wt%), FeO^T (1.24–2.61 wt%), and TiO_2 (0.26–0.29 wt%). In the TAS diagrams (Fig. 4a), all the samples are located in granite region, the Rock Crystal Differentiation Index（DI）is from 93.28 to 96.91, indicate that the samples are characterized by high differentiation. The Rittmann Indexes (σ) of the samples range from 2.36 to 2.81, in SiO_2-K_2O diagrams (Fig. 4b), all the samples are concentrated within the high-K calc-alkaline series field. The Alkalinity Ratio (AR) is 3.83–4.74, and the Aluminum Saturation Index (A/CNK) is 0.95–1.01. Results of the study suggest that these granites in the Zhangdaqi area are characterized by metaluminous-weak peraluminous (Fig. 4c).

All the samples have similar REE patterns. The total REE content (ΣREE) is 130.36–456.91 ppm, ratio of light rare earth elements to heavy rare earth elements (LREE/HREE) is 8.62–15.76 and $(La/Yb)_N$ is 7.57–18.67, showing that LREEs are relatively enriched, HREEs are relatively deficient and REE fractionation is obvious. All samples have $(La/Sm)_N$ = 3.87–6.58 and $(Gd/Yb)_N$ = 1.11–2.14, indicating that LREEs medium differentiation. They also have $(Gd/Lu)_N$=1.57–2.86, indicating that HREEs differentiation is weak. The δ_{Eu} values of samples is from 0.13 to 0.62, indicating that the samples are characterized by obvious negative Eu anomalies, suggest that the

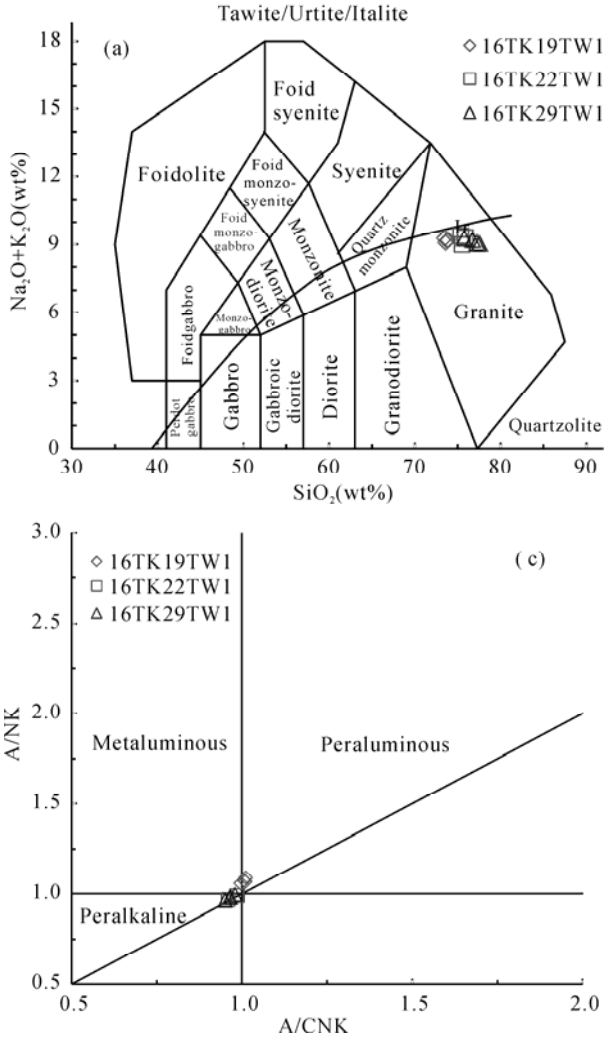


Fig. 4. (a) The TAS diagram (SiO_2 versus total alkali (Na_2O+K_2O)) (after Irvine and Baragar, 1971); (b) SiO_2 versus K_2O diagram (after Peccerillo and Taylor, 1976); (c)A/CNK versus A/NK diagram (after Maniar and Piccoli, 1989).

Table 1 Major (wt%) and trace (ppm) elements for the granites in the Zhangdaqi area

Sample No.	16TK19TW1				16TK22TW1			16TK29TW1			
	1	2	3	4	1	2	3	1	2	3	4
SiO_2	73.60	73.47	73.86	73.81	75.54	75.37	75.88	77.26	77.54	76.73	75.77
TiO_2	0.26	0.26	0.26	0.28	0.29	0.28	0.27	0.28	0.26	0.26	0.29
Al_2O_3	13.59	13.28	13.31	13.33	11.66	12.15	11.81	11.36	11.50	11.71	12.01
Fe_2O_3	1.12	1.19	1.15	1.41	2.24	1.77	1.84	1.47	1.28	1.59	1.92
FeO	0.88	0.92	0.72	0.66	0.59	0.46	0.73	0.27	0.10	0.21	0.26
MnO	0.06	0.06	0.05	0.05	0.04	0.05	0.03	0.04	0.04	0.03	0.05
MgO	0.54	0.12	0.08	0.12	0.05	0.07	0.10	0.11	0.14	0.13	0.14
CaO	0.53	0.42	0.39	0.45	0.01	0.03	0.06	0.09	0.11	0.09	0.11
Na_2O	4.66	4.47	4.42	4.44	3.63	3.75	3.75	3.47	3.43	3.51	3.55
K_2O	4.42	4.80	4.78	4.71	5.37	5.63	5.57	5.60	5.60	5.69	5.72
P_2O_5	0.05	0.05	0.05	0.06	0.02	0.01	0.02	0.02	0.02	0.01	0.02
LOI	0.50	0.66	0.68	0.68	0.62	0.59	0.36	0.34	0.51	0.35	0.52
FeO^T	1.89	1.99	1.76	1.92	2.61	2.06	2.39	1.59	1.24	1.64	1.99
Na_2O+K_2O	9.08	9.27	9.20	9.15	9.00	9.38	9.32	9.08	9.04	9.20	9.27
K_2O/Na_2O	0.95	1.08	1.08	1.06	1.48	1.50	1.48	1.61	1.63	1.62	1.61
$(Na_2O+K_2O)/CaO$	17.10	21.86	23.48	20.19	749.83	284.36	160.64	101.98	81.77	100.03	81.32
A/CNK	1.01	1.00	1.01	1.01	0.99	0.98	0.96	0.95	0.96	0.97	0.98
A/NK	1.09	1.06	1.07	1.07	0.99	0.99	0.97	0.96	0.98	0.98	1.00
DI	93.28	94.89	95.30	94.71	95.82	96.48	95.03	95.86	96.91	96.44	96.59
AR	4.61	4.74	4.65	4.62	4.28	4.21	4.43	4.08	3.89	3.93	3.83
δ	2.69	2.81	2.73	2.71	2.48	2.72	2.64	2.40	2.36	2.51	2.62
R1	2161	2143	2197	2192	2423	2318	2347	2554	2595	2484	2392
R2	351	315	310	318	234	246	243	238	244	246	255
Li	5.48	5.23	4.85	5.59	2.15	2.28	1.34	0.54	0.64	0.60	0.71
Be	2.94	2.82	2.71	2.89	3.97	3.17	2.40	1.10	0.99	1.09	1.21
Sc	2.38	2.37	1.90	2.79	3.16	3.02	1.49	1.62	1.73	1.23	1.82
Co	2.77	3.65	4.41	3.49	1.93	1.89	2.42	1.84	1.47	1.89	2.02
Cs	1.53	1.48	1.45	1.51	1.33	0.54	0.41	0.53	0.82	0.51	0.76
Hf	2.14	2.15	1.73	2.16	8.99	8.34	5.48	2.73	2.70	2.81	2.98
Ta	1.09	0.99	0.95	1.56	2.73	2.55	1.10	1.14	0.86	0.93	1.08
Tl	0.55	0.59	0.58	0.57	0.40	0.40	0.37	0.49	0.48	0.50	0.47
Th	10.31	12.69	11.65	12.77	11.56	11.55	9.57	7.97	7.05	7.27	7.00
U	3.81	2.26	2.90	1.96	2.85	2.88	2.02	1.30	1.52	1.26	1.56
Sn	2.29	2.03	2.25	2.07	2.60	2.63	2.35	2.93	2.77	1.77	1.91
Ba	523.5	516.4	520.8	495.6	180.9	137.3	128.8	141.9	148.2	161.3	145.4
Cr	12.0	18.1	22.1	32.2	28.8	20.3	15.1	24.1	33.0	19.1	26.3
Cu	3.70	3.71	5.29	4.77	4.52	3.39	4.77	28.67	17.64	33.79	22.28
Ga	18.63	17.47	17.33	18.41	23.75	26.01	24.97	22.11	22.64	22.21	23.48
Nb	19.05	19.49	17.62	18.67	25.88	22.80	24.37	18.22	17.27	17.10	18.45
Ni	1.9	2.0	1.9	2.0	1.2	1.0	1.1	0.7	0.7	0.6	0.8
Pb	17.3	18.2	18.4	18.4	22.2	19.7	17.3	19.3	22.9	20.7	72.0
Rb	119.7	127.2	124.8	124.5	89.1	95.8	89.6	96.9	95.0	98.7	97.5
Sr	151.5	145.6	144.4	148.4	32.8	20.7	30.4	24.6	24.3	25.4	23.1
V	17.5	17.0	17.0	19.1	11.8	11.1	7.1	10.5	11.0	8.3	12.2
Zn	25.2	22.8	19.0	23.2	101.1	97.3	75.8	47.8	66.8	43.6	67.4
Zr	188.6	199.0	186.7	205.3	522.1	435.9	432.7	415.4	399.5	391.9	404.1
Y	29.4	28.3	27.7	27.1	67.0	37.5	56.7	22.5	24.7	21.0	24.6
La	28.14	31.32	30.58	48.14	117.96	114.50	104.30	41.11	50.86	37.52	40.01
Ce	50.26	53.83	51.15	94.14	190.66	170.90	167.00	81.05	106.49	53.70	61.27
Pr	7.26	7.56	7.14	8.41	21.33	19.41	18.44	9.25	12.33	8.36	9.02
Nd	25.67	26.58	24.75	28.02	75.03	70.67	66.96	33.16	41.82	29.97	32.52
Sm	4.70	4.86	4.36	4.72	14.04	12.02	11.96	5.29	6.93	4.67	5.38
Eu	0.78	0.81	0.78	0.83	0.55	0.47	0.45	0.30	0.35	0.28	0.32
Gd	3.58	3.70	3.41	3.90	10.45	9.14	9.31	4.13	5.04	3.62	4.21
Tb	0.58	0.59	0.53	0.56	1.71	1.38	1.46	0.57	0.69	0.50	0.61
Dy	3.46	3.38	3.22	3.24	9.92	7.76	8.48	2.99	3.55	2.61	3.34
Ho	0.64	0.60	0.58	0.55	1.75	1.35	1.50	0.50	0.56	0.43	0.57
Er	2.04	1.82	1.82	1.72	5.39	4.15	4.42	1.47	1.63	1.29	1.68
Tm	0.32	0.29	0.29	0.26	0.79	0.64	0.65	0.21	0.24	0.19	0.24
Yb	2.67	2.37	2.43	2.17	6.61	5.37	5.29	1.79	1.95	1.64	2.08
Lu	0.28	0.25	0.25	0.23	0.72	0.58	0.58	0.20	0.22	0.18	0.23
ΣREE	130.36	137.96	131.29	196.91	456.91	418.35	400.78	182.02	232.66	144.96	161.47
LREE	116.81	124.96	118.76	184.26	419.57	387.98	369.11	170.16	218.78	134.49	148.51
HREE	13.56	12.99	12.54	12.65	37.34	30.38	31.68	11.86	13.88	10.47	12.96
LREE/HREE	8.62	9.62	9.47	14.56	11.24	12.77	11.65	14.35	15.76	12.84	11.46
δ_{Eu}	0.58	0.59	0.62	0.59	0.14	0.14	0.13	0.20	0.18	0.21	0.20
$(La/Yb)_N$	7.57	9.47	9.01	15.92	12.80	15.28	14.15	16.44	18.67	16.38	13.81
$(La/Sm)_N$	3.87	4.16	4.53	6.58	5.43	6.15	5.63	5.02	4.74	5.19	4.80
$(Gd/Yb)_N$	1.11	1.29	1.16	1.49	1.31	1.41	1.46	1.90	2.14	1.82	1.67
$(Gd/Lu)_N$	1.57	1.83	1.68	2.10	1.79	1.95	2.00	2.59	2.86	2.45	2.28

magma source area underwent plagioclase crystallization and differentiation. Characteristics of a right-slanted "V" (Fig. 5a) of samples is similar to the REE patterns of typical A-type granite. All the samples are relatively enriched in Rb, K, Th and depleted in Ba, Nb, Sr, P, Ti (Fig. 5b). The commonly observed Ba, Sr, P, and Ti depletions may be related to the fractional crystallizations of rutile, plagioclase and apatite in the magma source area.

4.2 Zircon LA-ICP-MS U-Pb dating

Zircon LA-ICP-MS U-Pb data for the granites in the Zhangdaqi area are showing in Table 2.

The zircons in monzogranite (16TK19TW1) of Dongfengshou are idiomorphic columnar, and the zircon crystals are 100–150 μm long. Ratios of the length and width range from 1.5:1 to 2:1, which present obvious oscillatory zoning (Fig. 6). Moreover, the zircons have a characteristic of typical magmatic zircon with Th/U ratios of 0.29–1.41. The isotope age of 25 zircon points falls on the concordia curve and its periphery (Fig. 7a), and the $^{206}Pb/^{238}U$ age between 291±3 Ma and 302±3 Ma. The weighted average is 297±1 Ma (MSWD=1.2).

The zircons in alkali-feldspar granite (16TK22TW1 and 16TK29TW1) and monzogranite (16TK28TW1) of Yilijiudui are idiomorphic columnar, the zircon crystals of alkali-feldspar granite are 90–150 μm long with length/width ratios of 1.2:1 to 2:1, the zircon crystals of monzogranite are 100–150 μm long with length/width ratios of 1.5:1 to 2:1. They all present obvious oscillatory zoning (Fig. 6). The zircons have high Th/U ratios (0.37–0.97) and present the characteristics of typical magmatic zircon. The isotope age of 24 zircon points in sample 16TK22TW1 falls on the concordia curve and its periphery (Fig. 7b). The $^{206}Pb/^{238}U$ age of 23 zircon points are from 290±3 Ma to 300±4 Ma, with the weighted average of 295±2 Ma (MSWD=1.3). The isotope age of 23 zircon points in sample 16TK29TW1 falls on the concordia curve and its periphery (Fig. 7d), and the $^{206}Pb/^{238}U$ age are from 288±3 Ma to 300±8 Ma. The weighted average is 294±1 Ma (MSWD=0.97). Sample 16TK28TW1 have analyzed 24 zircon points, except 3 points (16TK28TW1.7, 16TK28TW1.8, 16TK28TW1.17) with low degrees of concordance, the other 21 zircon points fall on the concordia curve and its periphery (Fig.

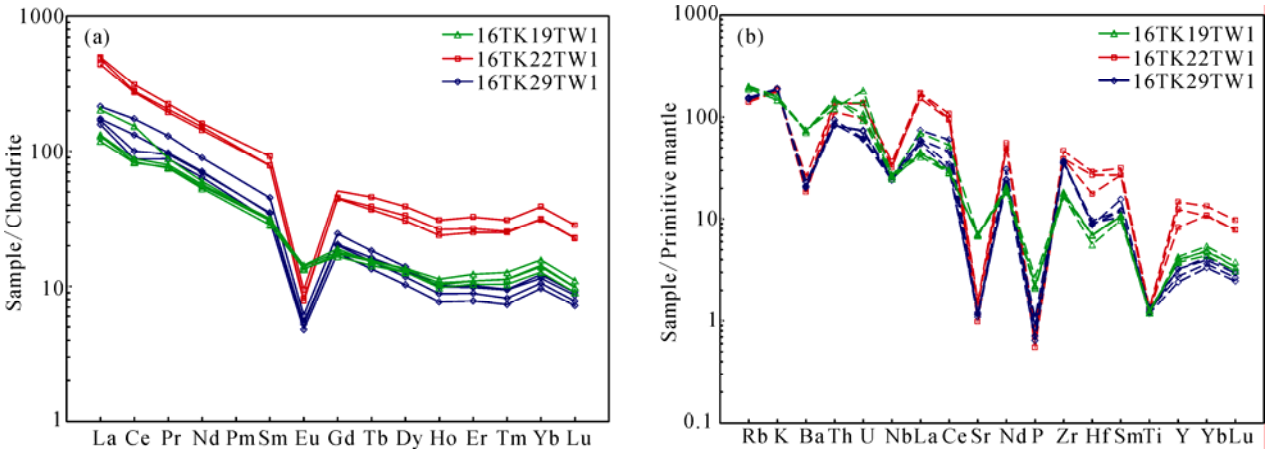


Fig. 5. (a) Chondrite-normalized REE patterns; (b) primitive-mantle-normalized multi-element diagrams (Normalizing values are from Sun and McDonough, 1989).

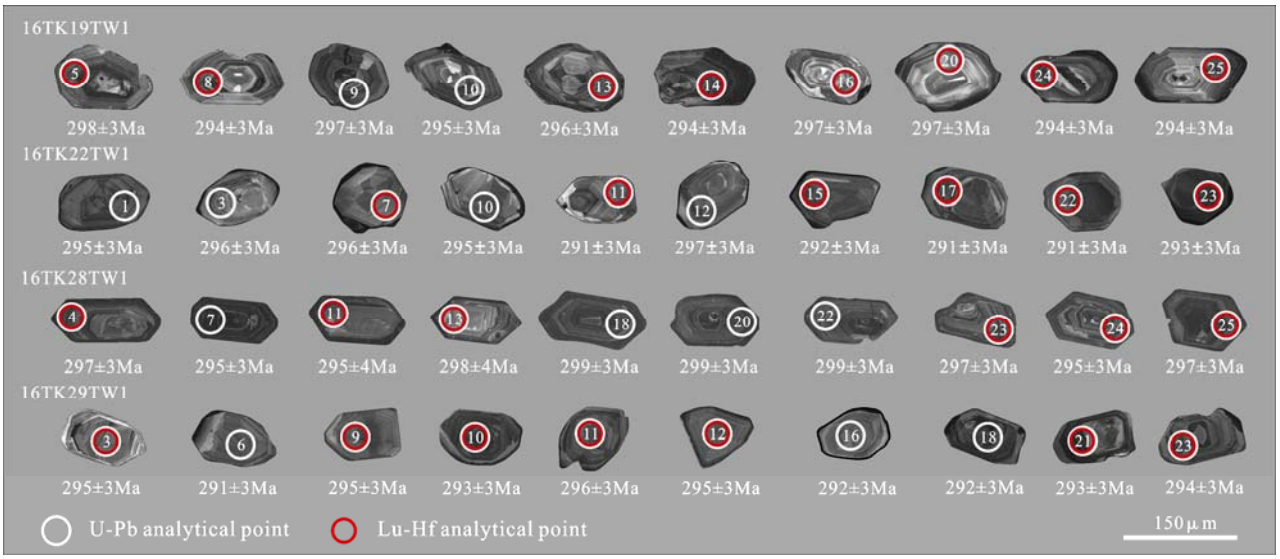


Fig. 6. The cathodoluminescence (CL) image of typical zircons from the granites in the Zhangdaqi area.

Table 2 Zircon LA-ICP-MS U-Pb data for the granites in the Zhangdaqi area

Spots	Element content (ppm)			Th/U	Isotope ratio				Age (Ma)			
	Pb	U	Th		$^{206}Pb/^{238}U$	1σ	$^{207}Pb/^{235}U$	1σ	$^{206}Pb/^{238}U$	1σ	$^{207}Pb/^{235}U$	1σ
16TK19TW1												
1	21	398	294	0.74	0.0479	0.0005	0.3539	0.0081	302	3	308	7
2	14	280	167	0.60	0.0478	0.0005	0.3546	0.0104	301	3	308	9
3	20	391	236	0.60	0.0479	0.0005	0.3551	0.0080	302	3	309	7
4	10	190	122	0.64	0.0478	0.0005	0.3457	0.0121	301	3	301	11
5	22	356	501	1.41	0.0473	0.0005	0.3453	0.0075	298	3	301	7
6	42	794	474	0.60	0.0478	0.0005	0.3567	0.0068	301	3	310	6
7	7	136	126	0.93	0.0463	0.0005	0.3385	0.0144	291	3	296	13
8	15	274	210	0.77	0.0467	0.0005	0.3452	0.0082	294	3	301	7
9	9	155	164	1.06	0.0472	0.0005	0.3483	0.0130	297	3	303	11
10	13	272	79	0.29	0.0468	0.0005	0.3431	0.0089	295	3	300	8
11	5	92	99	1.07	0.0471	0.0005	0.3478	0.0183	297	3	303	16
12	17	333	203	0.61	0.0467	0.0005	0.3391	0.0076	294	3	296	7
13	12	250	130	0.52	0.0470	0.0005	0.3449	0.0092	296	3	301	8
14	19	378	236	0.62	0.0466	0.0005	0.3425	0.0070	294	3	299	6
15	11	213	135	0.64	0.0471	0.0005	0.3439	0.0094	297	3	300	8
16	13	245	222	0.91	0.0472	0.0005	0.3474	0.0097	297	3	303	8
17	16	308	250	0.81	0.0476	0.0005	0.3455	0.0081	300	3	301	7
18	26	495	421	0.85	0.0476	0.0005	0.3477	0.0072	300	3	303	6
19	12	232	197	0.85	0.0475	0.0005	0.3392	0.0094	299	3	297	8
20	4	71	70	0.99	0.0472	0.0005	0.3470	0.0253	297	3	302	22
21	19	377	278	0.74	0.0462	0.0004	0.3386	0.0074	291	3	296	6
22	14	282	185	0.66	0.0465	0.0005	0.3375	0.0083	293	3	295	7
23	20	379	374	0.99	0.0463	0.0005	0.3453	0.0073	292	3	301	6
24	20	402	235	0.58	0.0467	0.0005	0.3433	0.0076	294	3	300	7
25	20	399	249	0.62	0.0467	0.0005	0.3372	0.0076	294	3	295	7
16TK22TW1												
1	11	234	99	0.42	0.0469	0.0005	0.3467	0.0071	295	3	302	6
2	14	284	118	0.42	0.0475	0.0005	0.3447	0.0080	299	3	301	7
3	17	351	160	0.46	0.0469	0.0005	0.3481	0.0067	296	3	303	6
5	13	272	108	0.40	0.0461	0.0005	0.3415	0.0077	290	3	298	7
6	17	361	153	0.42	0.0471	0.0005	0.3477	0.0068	297	3	303	6
7	9	191	74	0.39	0.0470	0.0005	0.3412	0.0098	296	3	298	9
8	16	335	165	0.49	0.0474	0.0005	0.3526	0.0074	298	3	307	6
9	11	229	86	0.37	0.0475	0.0005	0.3376	0.0085	299	3	295	7
10	10	199	92	0.46	0.0468	0.0005	0.3483	0.0091	295	3	303	8
11	10	204	87	0.42	0.0461	0.0005	0.3384	0.0087	291	3	296	8
12	13	266	112	0.42	0.0472	0.0005	0.3405	0.0078	297	3	298	7
13	14	287	147	0.51	0.0476	0.0005	0.3390	0.0079	300	3	296	7
14	12	258	120	0.46	0.0472	0.0005	0.3479	0.0081	297	3	303	7
15	11	230	102	0.44	0.0464	0.0005	0.3364	0.0077	292	3	294	7
16	12	239	110	0.46	0.0473	0.0005	0.3407	0.0089	298	3	298	8
17	15	315	135	0.43	0.0461	0.0005	0.3322	0.0071	291	3	291	6
18	9	179	80	0.44	0.0461	0.0005	0.3331	0.0109	291	3	292	10
19	10	223	106	0.48	0.0462	0.0005	0.3374	0.0095	291	3	295	8
20	10	218	82	0.37	0.0461	0.0005	0.3435	0.0098	290	3	300	9
21	10	209	97	0.46	0.0462	0.0005	0.3407	0.0084	291	3	298	7
22	6	129	52	0.40	0.0462	0.0005	0.3366	0.0141	291	3	295	12
23	7	155	61	0.39	0.0465	0.0005	0.3437	0.0101	293	3	300	9
24	11	258	108	0.42	0.0435	0.0005	0.3188	0.0077	275	3	281	7
25	26	548	233	0.42	0.0477	0.0006	0.3477	0.0070	300	4	303	6
16TK28TW1												
1	17	340	187	0.55	0.0478	0.0005	0.3501	0.0078	301	3	305	7
2	72	1364	998	0.73	0.0476	0.0005	0.3538	0.0061	300	3	308	5
4	42	856	408	0.48	0.0472	0.0005	0.3395	0.0062	297	3	297	5
5	30	538	290	0.54	0.0530	0.0005	0.3892	0.0069	333	3	334	6
6	45	882	652	0.74	0.0466	0.0005	0.3409	0.0056	293	3	298	5
7	85	1564	1325	0.85	0.0468	0.0005	0.5732	0.0102	295	3	460	8
8	41	734	326	0.44	0.0497	0.0005	0.5642	0.0116	313	3	454	9
9	28	574	257	0.45	0.0476	0.0006	0.3527	0.0074	300	4	307	6
10	13	261	150	0.58	0.0474	0.0005	0.3491	0.0078	299	3	304	7
11	23	449	265	0.59	0.0468	0.0006	0.3449	0.0072	295	4	301	6
12	68	1281	726	0.57	0.0480	0.0005	0.3500	0.0066	302	3	305	6
13	12	254	108	0.42	0.0473	0.0006	0.3408	0.0100	298	4	298	9
14	32	546	450	0.82	0.0519	0.0006	0.3809	0.0068	326	4	328	6
15	13	273	158	0.58	0.0461	0.0005	0.3417	0.0092	291	3	298	8
16	35	678	498	0.73	0.0477	0.0005	0.3540	0.0061	300	3	308	5
17	98	1455	1414	0.97	0.0520	0.0005	0.8283	0.0143	327	3	613	11
18	52	999	745	0.75	0.0475	0.0005	0.3468	0.0056	299	3	302	5
19	8	169	76	0.45	0.0469	0.0005	0.3339	0.0108	296	3	293	9
20	39	749	588	0.78	0.0475	0.0005	0.3423	0.0058	299	3	299	5
21	9	177	80	0.45	0.0472	0.0005	0.3406	0.0105	297	3	298	9

Continued Table 2

Spots	Element content (ppm)			Th/U	Isotope ratio				Age (Ma)			
	Pb	U	Th		$^{206}Pb/^{238}U$	1σ	$^{207}Pb/^{235}U$	1σ	$^{206}Pb/^{238}U$	1σ	$^{207}Pb/^{235}U$	1σ
22	26	531	306	0.58	0.0474	0.0005	0.3498	0.0063	299	3	305	5
23	44	879	523	0.60	0.0472	0.0005	0.3473	0.0058	297	3	303	5
24	56	1081	772	0.71	0.0469	0.0005	0.3428	0.0058	295	3	299	5
25	49	937	711	0.76	0.0472	0.0005	0.3420	0.0060	297	3	299	5
16TK29TW1												
1	15	298	150	0.50	0.0473	0.0005	0.3423	0.0078	298	3	299	7
2	14	279	139	0.50	0.0471	0.0005	0.3439	0.0080	296	3	300	7
3	13	256	109	0.43	0.0469	0.0005	0.3436	0.0085	295	3	300	7
4	19	363	208	0.57	0.0476	0.0005	0.3509	0.0075	300	3	305	7
5	10	204	71	0.35	0.0473	0.0005	0.3497	0.0109	298	3	305	9
6	11	225	109	0.48	0.0462	0.0005	0.3363	0.0096	291	3	294	8
7	12	234	108	0.46	0.0471	0.0005	0.3422	0.0097	297	3	299	9
9	13	269	132	0.49	0.0469	0.0005	0.3359	0.0082	295	3	294	7
10	13	264	146	0.55	0.0464	0.0005	0.3353	0.0074	293	3	294	6
11	10	202	91	0.45	0.0470	0.0005	0.3490	0.0095	296	3	304	8
12	13	257	153	0.60	0.0468	0.0005	0.3423	0.0084	295	3	299	7
13	12	240	144	0.60	0.0463	0.0005	0.3403	0.0078	292	3	297	7
14	10	209	105	0.50	0.0467	0.0005	0.3363	0.0083	294	3	294	7
15	13	273	180	0.66	0.0461	0.0005	0.3337	0.0081	290	3	292	7
16	14	287	168	0.59	0.0463	0.0005	0.3406	0.0085	292	3	298	7
17	12	240	133	0.56	0.0464	0.0005	0.3458	0.0082	292	3	302	7
18	25	493	371	0.75	0.0463	0.0005	0.3426	0.0065	292	3	299	6
19	13	270	178	0.66	0.0460	0.0005	0.3405	0.0081	290	3	298	7
20	13	260	166	0.64	0.0457	0.0005	0.3335	0.0080	288	3	292	7
21	8	157	77	0.49	0.0464	0.0005	0.3447	0.0121	293	3	301	11
23	10	211	107	0.51	0.0466	0.0005	0.3466	0.0090	294	3	302	8
24	7	138	65	0.47	0.0473	0.0005	0.3531	0.0127	298	3	307	11
25	11	228	111	0.49	0.0468	0.0005	0.3404	0.0103	295	3	297	9

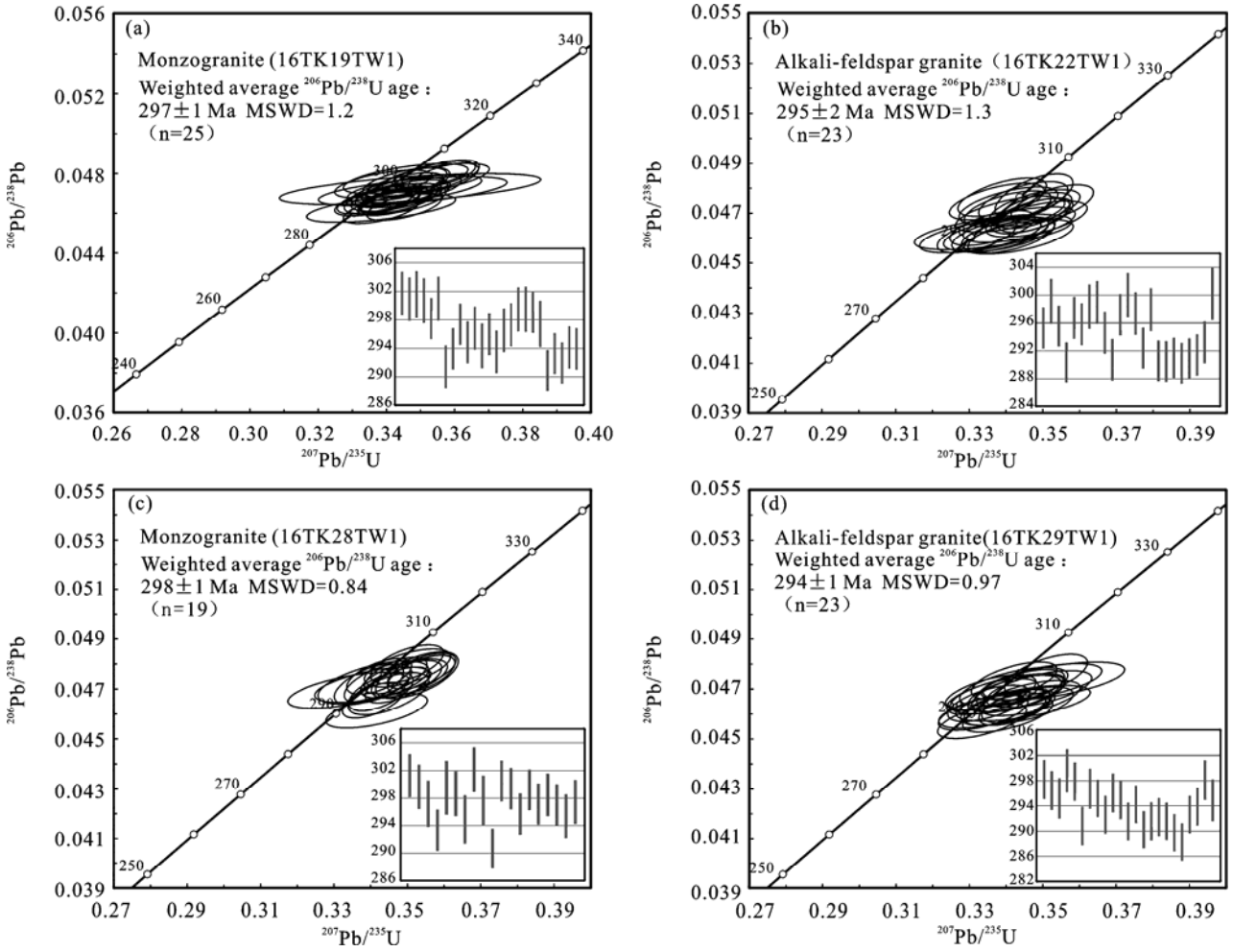


Fig. 7. Zircon U-Pb age concordia diagrams and weighted average age of the granites in the Zhangdaqi area.

7c). The $^{206}Pb/^{238}U$ age of 19 points are from 291±3 Ma to 302±3 Ma, with the weighted average of 298±1 Ma (MSWD=0.84). However, the $^{206}Pb/^{238}U$ ages of 2 points (16TK28TW1.5, 16TK28TW1.14) are 333±3 Ma and 326±4 Ma, and they are maybe the age of captured zircon when the magma is rising.

4.3 Zircon Lu-Hf Isotopic

We analyzed zircon Lu-Hf isotope after U-Pb isotopic dating, detailed data are showing in Table 3.

48 zircon Lu-Hf analytical points were performed on granite samples (16TK19TW1, 16TK22TW1, 16TK28TW1 and 16TK29TW1). Two points (16TK28TW1.15, 16TK29TW1.23) data are abandoned because they have unreasonable two-stage model age (83 Ma and 187 Ma) which is much smaller than granite crystallization age. It may be caused by the analysis error. Most points $^{176}Lu/^{177}Hf$ ratios are less than 0.002 except 13 points, total average is of 0.0018, and this expresses that the zircons have lower accumulation of radiogenic Hf in the process of rock formation, so we could explore genetic information of the granites by zircon $^{176}Hf/^{177}Hf$ ratios (Stille and Steiger, 1991; Wu et al., 2007). All points $f_{Lu/Hf}$ values are between −0.97 and −0.90, which is lower than those of mafic crust (−0.34) and felsic crust (−0.72) (Amelin et al., 1999). Therefore, the two-stage model age better reflects the timing of the extraction of source material from the depleted mantle or the residence time of source material in crust.

All samples (16TK19TW1, 16TK22TW1, 16TK28TW1

Table 3 Zircon Lu-Hf isotope data for the granites in the Zhangdaqi area

Spots	Age (Ma)	$^{176}Yb/^{177}Hf$	$^{176}Lu/^{177}Hf$	$^{176}Hf/^{177}Hf$	2σ	$\varepsilon_{Hf}(t)$	T_{DM1} (Ma)	T_{DM2}(Ma)	$f_{Lu/Hf}$
16TK19TW1									
5	298	0.0410	0.0017	0.282899	0.000019	10.7	510	768	−0.95
8	294	0.0372	0.0016	0.282885	0.000016	10.2	528	815	−0.95
12	294	0.0312	0.0014	0.282892	0.000019	10.4	516	791	−0.96
13	296	0.0370	0.0015	0.282892	0.000017	10.4	518	791	−0.95
14	294	0.0351	0.0015	0.282868	0.000016	9.6	552	869	−0.95
15	297	0.0241	0.0010	0.282888	0.000016	10.4	517	793	−0.97
16	297	0.0423	0.0018	0.282939	0.000021	12.1	453	642	−0.95
20	297	0.0317	0.0014	0.282864	0.000023	9.5	556	876	−0.96
21	291	0.0239	0.0010	0.282905	0.000018	11	493	747	−0.97
22	293	0.0343	0.0015	0.282864	0.000017	9.4	558	883	−0.95
24	294	0.0380	0.0017	0.282944	0.000027	12.2	446	631	−0.95
25	294	0.0344	0.0016	0.282854	0.000017	9.1	573	915	−0.95
16TK22TW1									
5	290	0.0510	0.0019	0.283003	0.000022	14.2	362	449	−0.94
7	296	0.0465	0.0019	0.282892	0.000026	10.4	523	796	−0.94
11	291	0.0434	0.0017	0.282926	0.000025	11.5	470	689	−0.95
15	292	0.0412	0.0016	0.282949	0.000026	12.4	437	615	−0.95
17	291	0.0442	0.0016	0.282934	0.000022	11.8	458	663	−0.95
18	291	0.0503	0.0020	0.282957	0.000023	12.6	429	595	−0.94
19	291	0.0491	0.0018	0.282936	0.000023	11.9	458	660	−0.94
20	290	0.0525	0.0019	0.282941	0.000020	12.0	452	647	−0.94
21	291	0.0401	0.0016	0.282932	0.000025	11.8	460	668	−0.95
22	291	0.0315	0.0012	0.282886	0.000029	10.2	523	811	−0.96
23	293	0.0632	0.0023	0.282933	0.000026	11.7	469	677	−0.93
24	275	0.0731	0.0026	0.282937	0.000025	11.4	466	689	−0.92
16TK28TW1									
2	300	0.0578	0.0022	0.282942	0.000020	12.2	454	636	−0.93
4	297	0.0994	0.0033	0.282937	0.000022	11.7	477	678	−0.90
6	293	0.0479	0.0018	0.282902	0.000019	10.7	508	768	−0.94
9	300	0.0381	0.0014	0.282883	0.000024	10.2	530	813	−0.96
11	295	0.0468	0.0017	0.282900	0.000017	10.7	510	771	−0.95
13	298	0.0304	0.0012	0.282878	0.000019	10.1	534	828	−0.96
15	291	0.0553	0.0020	0.283117	0.000034	18.2	196	83	−0.94
19	296	0.0450	0.0017	0.282858	0.000022	9.2	570	904	−0.95
21	297	0.0508	0.0019	0.282952	0.000022	12.5	437	605	−0.94
23	297	0.0580	0.0022	0.282936	0.000025	11.9	464	661	−0.93
24	295	0.0692	0.0025	0.282970	0.000023	13.0	417	560	−0.92
25	297	0.0729	0.0026	0.282973	0.000024	13.1	412	547	−0.92
16TK29TW1									
1	298	0.0607	0.0016	0.282904	0.000039	10.9	501	750	−0.95
2	296	0.0667	0.0017	0.282863	0.000041	9.4	563	889	−0.95
3	295	0.1009	0.0026	0.282995	0.000046	13.8	381	482	−0.92
7	297	0.0871	0.0022	0.282926	0.000043	11.5	478	693	−0.93
9	295	0.0743	0.0018	0.282978	0.000041	13.4	398	522	−0.94
10	293	0.0904	0.0022	0.282869	0.000044	9.4	561	880	−0.93
11	296	0.0771	0.0019	0.282848	0.000044	8.8	587	939	−0.94
12	295	0.0880	0.0021	0.282837	0.000034	8.4	606	977	−0.94
14	294	0.0858	0.0021	0.282944	0.000039	12.1	450	636	−0.94
21	293	0.0434	0.0012	0.282897	0.000037	10.6	507	773	−0.96
23	294	0.0746	0.0018	0.283082	0.000042	17.1	245	187	−0.94
25	295	0.0829	0.0022	0.282886	0.000036	10.1	536	822	−0.93

and 16TK29TW1) have relatively high $^{176}Hf/^{177}Hf$ values. The $\varepsilon_{Hf}(t)$ values are 9.1–12.2, 10.2–14.2, 9.2–13.1, 8.4–13.8. The two-stage model age of granite samples are 631–915 Ma, 449–811 Ma, 547–904 Ma, 482–977 Ma, representing the Early Paleozoic-Neoproterozoic magmatic source. In summary, the zircon Lu-Hf isotopic data indicate that the granites in the Zhangdaqi area is characterized by positive $\varepsilon_{Hf}(t)$ values and relatively young two-stage model age.

5 Discussions

5.1 Formation age of the granites

A large amount of the granites are exposed in the northern side of Hegenshan-Heihe Suture. According to the U-Pb isotope dating results, some scholars believe that the crystallization age of the granites are Late Carboniferous (299–317 Ma) (Qu et al., 2011; Zhang et al.,2011; Cheng et al.,2012; Zhao et al., 2013; Kong et al.,2017; Yang et al.,2017; Wang et al.,2017; Shi et al.,2019). However, we measured the crystallization age of the granites in the Zhangdaqi area is Early Permian (294–298 Ma). In addition, other scholars have also reported the age of the Early Permian granites along the Hegenshan-Heihe Suture. For instance, zircon U-Pb age of moyite in Shierzhan area is 298±2 Ma (Sui et al.,2009), zircon U-Pb age of alkali-feldspar granites from Sizhanlinchang, Xiaoshantun and Daheishan in Nenjiang County are 282±4 Ma, 285±2 Ma and 292±4 Ma (Wu et al.,2002), zircon U-Pb age of alkali-feldspar granite in Heihe area is 292±4 Ma (Guo et al., 2011), zircon U-Pb age of alkali-feldspar granite from Hanbuyinbudun in East Ujimqin Banner is 295.1±2.8 Ma (Liu, 2009), zircon U-Pb isotopic age of alkali granite from Jinggesitai in East Ujimqin Banner is 284.8±1.1 Ma (Zhang et al.,2009). All above data indicate that there's a granites belt along Hegenshan-Heihe Suture, and the formation age is Late Carboniferous -Early Permian (~320–280 Ma) (Fig. 8), the granites in the Zhangdaqi area are belonging to this granites belt.

5.2 Petrogenesis and source properties

The original A-type granite was defined as granitic rocks with alkaline, anhydrous characteristics (Loiselle and Wones, 1979). High water content in A-type granite was explained well when the aluminum A-type granite has been put forward (King et al., 1997). Zhang et al. (2012) summarized the essence of A-type granite, that it was partially melted granite at low pressure, and was characterized distinctly by high-K (K_2O content 4–6 wt% or higher). The granite also contain swan distribution REE

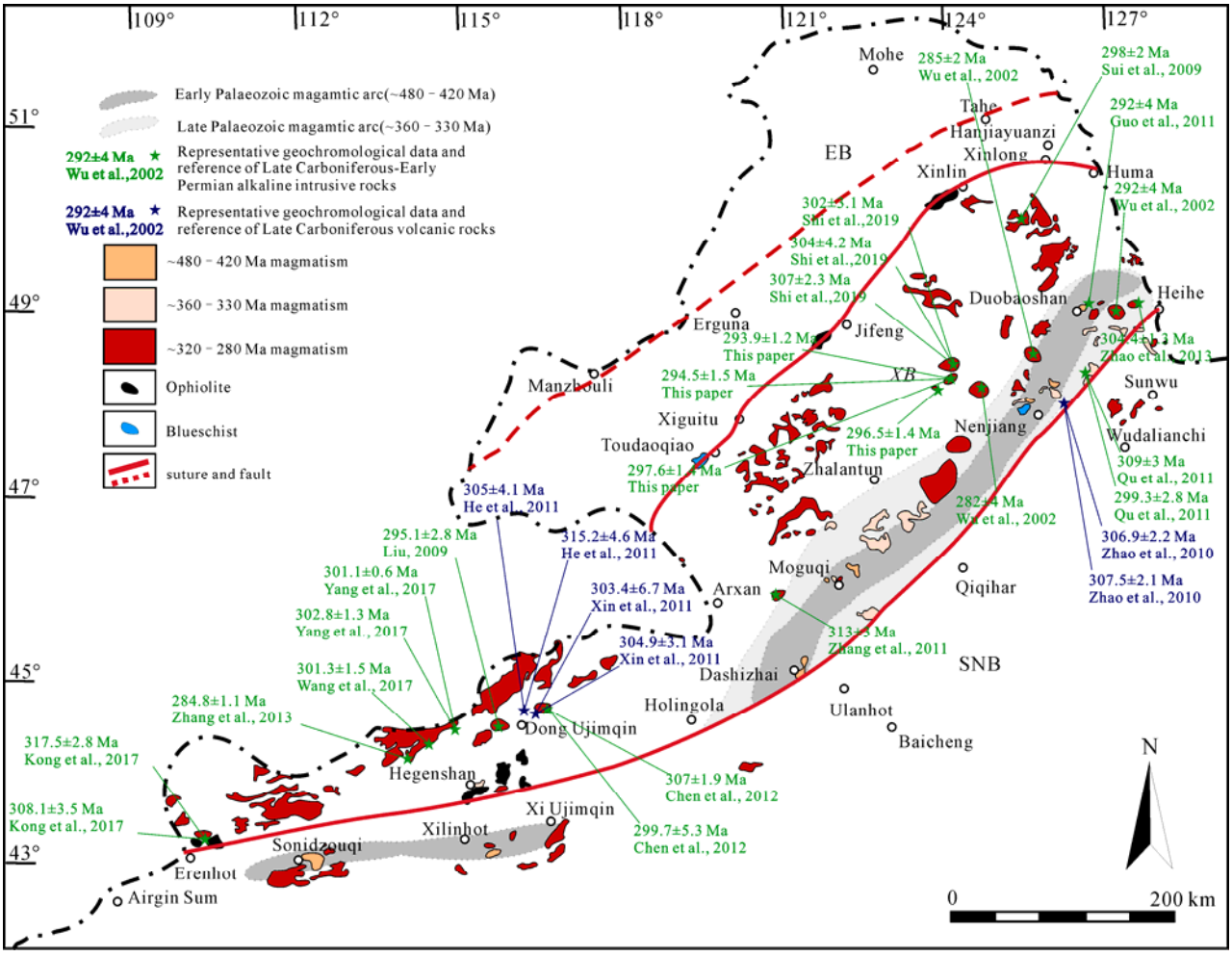


Fig. 8. Late Carboniferous-Early Permian igneous rocks age distribution diagrams along Hegenshan-Heihe Suture (after Liu et al., 2017).

patterns, and depleted in Eu, Ba, Sr, P and Ti. King et al. (1997) explained the concept of the aluminum A-type granite of plutons from Lachlan fold belt in Australia. The primary features of those granites are high-Al (Al_2O_3 content greater than 12 wt%), A/CNK values greater than 1 (Zhou, 2011). The major elements of monzogranite and alkali-feldspar granite in the Zhangdaqi area are characterized by high-Si (SiO_2 is 73.47–77.54 wt%) and high-K (K_2O is 4.42–5.72 wt%). Al_2O_3 content is 11.36–13.59 wt% and A/CNK ratios is 0.95–1.01. Trace elements have an obvious negative Eu anomaly, and rich in Rb, K and Th, loss in Ba, Sr, P and Ti. These major and trace elements characteristics suggest that the granites in the Zhangdaqi area are the aluminum A-type granite. In the discriminant diagrams of granite genetic types (Fig. 9), alkali-feldspar granite in the Zhangdaqi area is plotted into A-type granite region, but monzogranite fall in I&S-type granite region. However, 10000Ga/Al ratios of monzogranite is 2.46–2.61 with the average of 2.54, Significantly higher than the average of S-type (2.28) and I-type (2.1) granites (Whalen et al., 1987), the geochemical characteristics of monzogranite make clear that it is A-type granite. Zr content of A-type granites would be decreasing when they experienced intense crystallization differentiation, so A-type granites show the characteristics of high differentiation I-type granite (Wu et al., 2007). This explains why monzogranite fall in I&S-type granite region (Fig. 9).

In terms of magmatic rocks, the composition of zircon Lu-Hf isotopic provide definitive evidence for identification of magma source and the specific process of magma evolution (Wu et al., 2007). A-type granites in the Zhangdaqi area have positive $\varepsilon_{Hf}(t)$ values (8.4–14.2), with an average value of 11.1. They mainly fell along the chondrite-depleted mantle evolution lines and within the $\varepsilon_{Hf}(t)$ range of Phanerozoic igneous rocks in the eastern segment of the CAOB (Fig. 10a) (Xiao et al., 2004; Chen et al., 2009). The zircon Hf isotope compositions in the granites from the Zhangdaqi area is very similar, suggesting that they come from the same magma source area. The two-stage model age (T_{DM2}) is between 449 Ma and 977 Ma (Early Paleozoic-Neoproterozoic), which

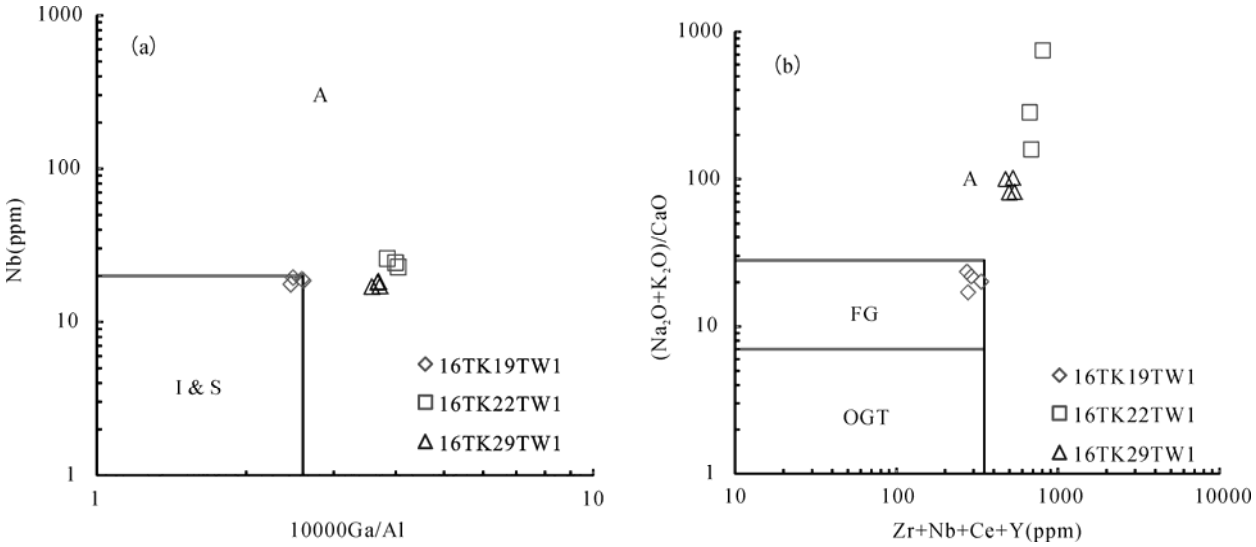


Fig. 9. (a) Nb versus 10000Ga/Al diagram (after Whalen et al., 1987); (b) $(Na_2O+K_2O)/CaO$ versus Zr+Nb+Ce+Y diagram (after Whalen et al., 1987).

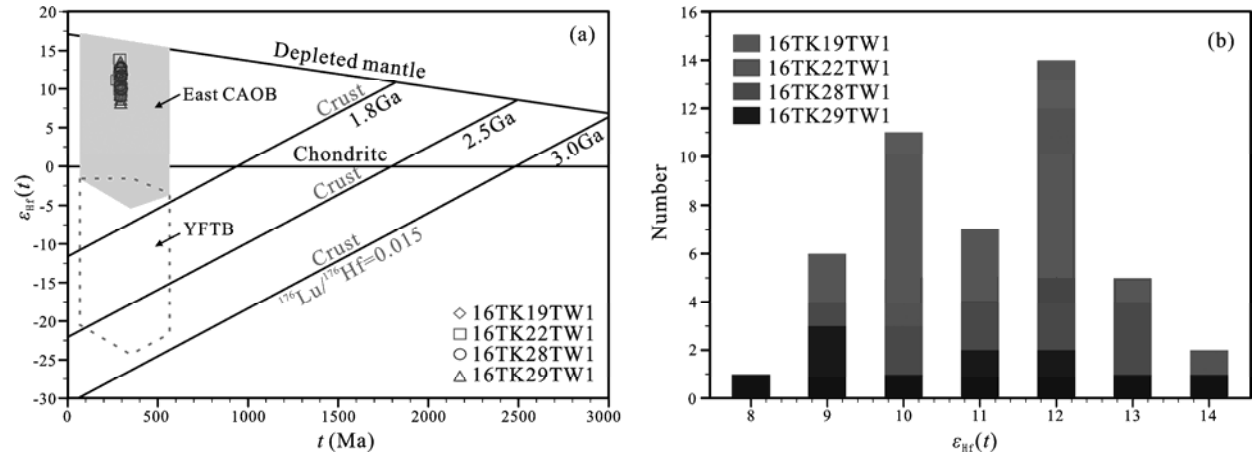


Fig. 10. (a) Compilation diagram of $\varepsilon_{Hf}(t)$ vs. U-Pb ages of the granites in the zhangdaqi area (after Wu et al., 2007); (b) Histogram of $\varepsilon_{Hf}(t)$ values of zircons.

indicates that the magma forming the A-type granites at the Zhangdaqi area was generated by the re-melting of the Early Paleozoic-Neoproterozoic juvenile crust.

A-type granites in the Zhangdaqi area have Nb/Ta ratios of 9.0–22.2, and the average value is 16.3, which is closed to the ratios (17.5) in mantle-derived magma (Sun and McDonough, 1989), the Zr/Hf ratios of these granites is between 52.3 to 152.0, which is much higher than the value (33) in crust-derived magma (Taylor and McLennan, 1985) and relatively close to the value (39) in mantle-derived magma (McDonough and Sun, 1995), suggesting that mantle-derived components mixed into the magma. Therefore, A-type granites in the Zhangdaqi area are produced by partially molten material in the lower crust and mantle source material.

5.3 Tectonic setting

According to the tectonic setting of A-type granite, it is generally believed that the granites formed in extensional environment (Pitcher, 1993). Eby (1992) divided A-type granite into A1 and A2 subtypes. A1 type granite mainly formed in continental-rift and intraplate environment, while A2 type granite usually formed in extensional environment after collision. In the Nb-Y-3Ga diagrams (Fig. 11c) and the Nb-Y-Ce diagrams (Fig. 11d), A-type granites in the Zhangdaqi area all fall in A2 type granite region, combined with trace element characteristics, these granites are relatively enriched in Rb, K, Th and depleted in Ba, Nb, Sr, P, Ti, indicating typical characteristics of continental magmatic arc. In Rb-(Yb+Nb) diagrams (Fig. 11a), most of these granites fall in volcanic-arc granite (VAG) region. In R1-R2 diagrams (Fig. 11b), A-type granites in the Zhangdaqi area were located in a post-orogenic environment.

5.4 Geological implication

There are many views on the amalgamation time of Xing'an and Songnen Blocks, such as the Late Silurian-Devonian (Sengor et al., 1996), late Early Carboniferous (Zhao et al., 2010), before the Permian (Shi et al., 2004;

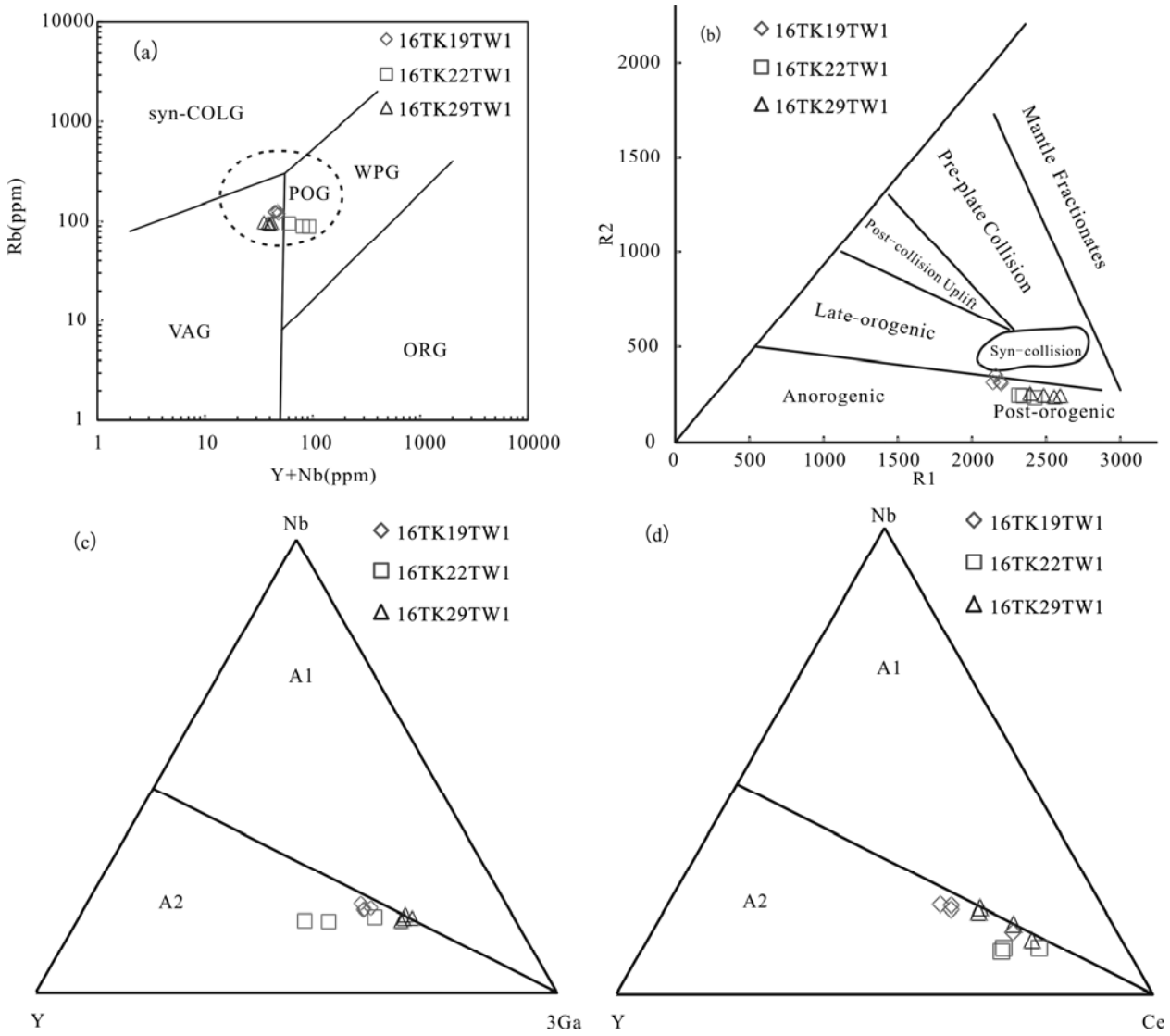


Fig. 11. (a) Rb versus Y+Nb diagram (after Pearce et al., 1984); (b) R1-R2 diagram (after Batchelor and Bowden, 1985); (c) Nb -Y-3Ga diagrams (after Eby, 1992); (d) Nb-Y-Ce diagrams (after Eby, 1992).

Tong et al., 2010) and Triassic (Chen et al., 2000; Miao et al., 2004; Li et al. 2016, 2017). At present, most scholars support that the combination of the two blocks occurred in the Late Paleozoic. Liu et al. (2017) suggested that this region contains two subduction-related magmatic arcs along the eastern margin of the Xing'an Block that formed at ~480–420 Ma and ~360–330 Ma (Fig. 8), and the amalgamation of Xing'an and Songnen Blocks is a long-term process.

In recent years, lots of U-Pb isotopic ages of A-type granites have been reported from north to south along the Hegenshan-Heihe Suture. Sui et al. (2009) reported that the age of moyite in Shierzhan is 298±2 Ma, Zhao et al. (2013) reported that the age of syenogranite from Dayinhe in Heihe is 304.4±1.3 Ma. Guo et al. (2011) reported that the age of alkali-feldspar granite in Heihe is 292±4 Ma. Wu et al. (2002) reported that the age of alkali-feldspar granite in Sizanlinchang and Xiaoshantun are 282±4 Ma and 285±2 Ma, and alkali granite in Daheishan is 292±4 Ma. Qu et al. (2011) reported that the age of alkali-feldspar granite and syenogranite in Duobaoshan are 309±3 Ma and 299.3±2.8 Ma. Shi et al. (2019) reported that the age of alkali-feldspar granite from Yili is 302±3.1 Ma, 304±4.2 Ma and 307±2.3 Ma. Zhang et al. (2011) reported that the age of monzogranite in Taerqi is 313±3 Ma. Cheng et al. (2012) reported that the age of monzogranite and syenogranite from Henmaiwenduer in East Ujimqin Banner are 307±1.9 Ma and 299.7±5.3 Ma. Liu (2009) reported that the age of alkali-feldspar granite from Hanbuyinbudun in East Ujimqin Banner is 295.1±2.8 Ma. Yang et al. (2017) reported that the age of monzogranite and alkali granite in Baiyintuga are 302.8±1.3 Ma and 301.1±0.6 Ma. Wang et al. (2017) reported that the age of alkali granite from Jinggesitai in East Ujimqin Banner is 301.3±1.5 Ma. Zhang et al., (2009) reported that the age of alkali granite from Jinggesitai in East Ujimqin Banner is 284.8±1.1 Ma. Kong et al. (2017) reported that the age of syenogranite from Halatumiao pluton and biotite monzonitic granite from Saiyinwusu pluton in Enerhot are 317.5±2.8 Ma and 308.1±3.5 Ma. These ages mainly focus on Late Carboniferous-Early Permian (Fig. 8, Table 4).

Zhao et al. (2010) reported the age of tuffaceous rhyolite and rhyolitic crystalline tuff of the Baoligaomiao Formation in Duobaoshan are 306.9±2.2 Ma and 307.5±2.1 Ma, Xin et al. (2011) reported the age of rhyolite and quartz crystalline tuff of the Baoligaomiao Formation in East Ujimqin Banner are 303.4±6.7 Ma and 304.9±3.1 Ma. He et al. (2017) reported the age of eutectic rhyolite and rhyolite of the Baoligaomia Formation from Bayanaobao in East Ujimqin Banner are 305±4.1 Ma and 315.2±4.6 Ma. These ages mainly focus on Late Carboniferous (Fig. 8, Table 4). Bimodal volcanic rocks and A-type granites formed in extensional environment (Xue et al., 2010; Zhang et al., 2012; Shao et al., 2014), and this indicates that Hegenshan-Hehei Suture is in a post-orogenic extensional environment in the Late Carboniferous-Early Permian. Zhou et al. (2015) believed that Hegenshan ophiolite formed between 300 Ma and 335 Ma, suggesting that the closure of the ocean between Xing'an and Songnen Blocks occurred between early Early Carboniferous and Late Carboniferous.

The Zhangdaqi area is located in north of the Hegenshan-Heihe Suture. In the convergence process of the ocean between Xing'an and Songnen Blocks, the subducted slab was broken off. Large-scale underplating of mantle-derived magma occurred along the crust-mantle boundary and caused the partial melting of lower crustal materials, and then mixed with the mantle-derived magma, formed the parent magma of the A-type granites and

Table 4 Chronological data for the Late Paleozoic igneous rocks along Hegenshan-Heihe Suture

Rocktypes	Order	Sample	Location	Lithology	Age(Ma)	Method	Reference
Granitoids	1	14SNT-07	Enerhot	Syenogranite	317.5±2.8	LA-ICP-MS	Kong et al.,2017
	2	14SNT-10	Enerhot	Biotite monzonitic granite	308.1±3.5	LA-ICP-MS	Kong et al.,2017
	3	GW04249	Taerqi	Monzogranite	313±3	LA-ICP-MS	Zhang et al.,2011
	4	TW21	Yili	Alkali-feldspar granite	307±2.3	SHRIMP	Shi et al.,2019
	5	TW8	Yili	Alkali-feldspar granite	304±4.2	SHRIMP	Shi et al.,2019
	6	B-b5	Yili	Alkali-feldspar granite	302±3.1	SHRIMP	Shi et al.,2019
	7	1020-1	Henmaiwenduer	Monzogranite	307±1.9	SHRIMP	Cheng et al.,2012
	8	0058-1	Henmaiwenduer	Syenogranite	299.7±5.3	SHRIMP	Cheng et al.,2012
	9	HZTW05	Dayinhe	Syenogranite	304.4±1.3	LA-ICP-MS	Zhao et al.,2013
	10	0567	Duobaoshan	Alkali-feldspar granite	309±3	SHRIMP	Qu et al.,2011
	11	1411	Duobaoshan	Syenogranite	299.3±2.8	SHRIMP	Qu et al.,2011
	12	14SJ43	Jinggesitai	Alkali granite	301.3±1.5	LA-ICP-MS	Wang et al.,2017
	13	HQ042	Baiyintuga	Monzogranite	302.8±1.3	LA-ICP-MS	Yang et al.,2017
	14	HG050	Baiyintuga	Alkali-feldspar granite	301.1±0.6	LA-ICP-MS	Yang et al.,2017
	15	GW05157	Shierzhan	Moyite	298±2	LA-ICP-MS	Sui et al.,2009
	16	JG21-60-104	Hanbuyinbudun	Alkali-feldspar granite	295.1±2.8	LA-ICP-MS	Liu,2009
	17	Jan-43	Daheishan	Alkali granite	292±4	LA-ICP-MS	Wu et al.,2002
	18	Jan-01	Xiaoshantun	Alkali-feldspar granite	285±2	LA-ICP-MS	Wu et al.,2002
	19	Feb-05	Sizhanlinchang	Alkali-feldspar granite	282±4	LA-ICP-MS	Wu et al.,2002
	20	P15TC57	Heihe	Alkali-feldspar granite	292±4	LA-ICP-MS	Guo et al.,2011
	21	3TW5129-1	Jinggesitai	Alkali granite	284.8±1.1	U-Pb isotopic dilution method	Zhang et al.,2009
Volcanic rocks	1	HH32-82	Duobaoshan	Ruffaceous rhyolite	306.9±2.2	LA-ICP-MS	Zhao et al.2010
	2	HH6-15	Duobaoshan	Rhyolitic crystalline tuff	307.5±2.1	LA-ICP-MS	Zhao et al.2010
	3	T1542-1	Dongwuqi	Rhyolite	303.4±6.7	SHRIMP	Xin et al.2011
	4	TW3086-1	Dongwuqi	Quartz crystalline tuff	304.9±3.1	SHRIMP	Xin et al.2011
	5	PM012-8	Bayanaobao	Eutectic rhyolite	305±4.1	LA-ICP-MS	He et al.2017
	6	B012	Bayanaobao	Rhyolite	315.2±4.6	LA-ICP-MS	He et al.2017

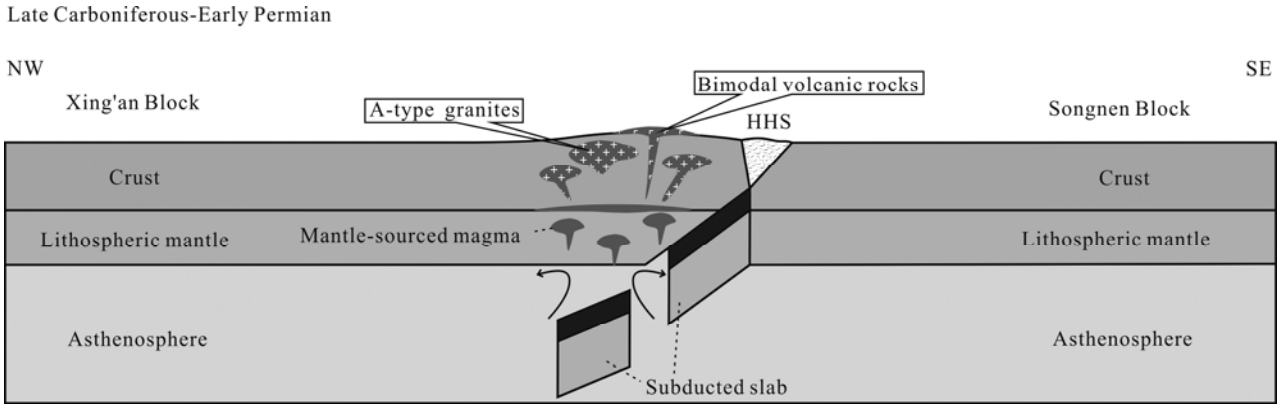


Fig. 12. Schematic model showing the Late Carboniferous-Early Permian tectonic evolution and genesis of magma.

bimodal volcanic rocks along the Hegenshan-Heihe Suture during the Late Carboniferous-Early Permian (Fig. 12). A-type granites in the Zhangdaqi area formed in this post-orogenic extensional environment.

6 Conclusions

(1) The granites in the Zhangdaqi area are characterized by metaluminous-weak peraluminous and high-K calc-alkaline series. The trace elememts of these granites show that LREEs are relatively enriched, while HREEs are relatively deficient and REE fractionation is obvious. Those granites are characterized by obvious negative Eu anomalies, meanwhile, they are relatively enriched in Rb, K, Th and depleted in Ba, Nb, Sr, P, Ti. All of these suggest that these granites in the Zhangdaqi area are aluminum A-type granite.

(2) The crystallization age of the granites in the Zhangdaqi area are 294-298 Ma, indicating their formation age is Early Permian. All these granites are A-type granite that formed in the post-orogenic extensional environment. The magmatic source area is a mixture of partial melting of the lower crust and depleted mantle.

(3) A-type granites and bimodal volcanic rocks along the Hegenshan-Heihe Suture formed during the Late Carboniferous-Early Permian, indicating that the HHS between Xing'an and Songnen Blocks closed in the late Early-Carboniferous. Subsequently, the Zhangdaqi area was in a post-orogenic extensional environment from Late Carboniferous to Early Permian and resulted in the formation of the A-type granites.

Acknowledgments

This study is supported by China Geological Survey Project (Grant NO. DD20160047-02, DD20190042-03) and National Key Research and Development Program (Grant NO. 2017YFC0601300-01, 2017YFC0601401, 2017YFC 0601305-02) and Qingdao Leading innovation talents project (19–3–2–19–zhc). Thanks to review experts and editors for their valuable amendments and suggestions. Thanks to Isotopic Laboratory, Tianjin Institute of Geology and Mineral Resources for their help in the zircon LA-ICP-MS U-Pb dating and Lu-Hf isotope analysing. Thanks to Northeast Mineral Resources and Supervision Testing Center, Ministry of Land and Resources for their assistance in geochemical analyses.

Manuscript received May 15, 2019
accepted Aug. 14, 2019
associate EIC XIAO Wenjiao
edited by LIU Lian

References

Amelin, Y., Lee, D.C., Halliday, A.N., and Pidgeno, R.T., 1999. Nature of the Earth's earliest crust from hafnium isotopes in single detrital zircons. Nature, 399: 252–255.

Amelin, Y., and Davis, W.J., 2005. Geochemical test for branching decay of ^{176}Lu. Geochimica et Cosmochimica Acta, 69(2): 465–473.

Batchelor, R.A., and Bowden, P., 1985. Petrogenetic interpretation of granitoid rock series using multicationic parameters. Chemical Geology, 48(1): 43–55.

Bouvier, A., Vervoort, J.D., and Patchett, P.J., 2008. The Lu-Hf and Sm-Nd isotopic composition of CHUR: Constrains from unequilibrated chondrites and implications for the bulk composition of terrestrial planets. Earth and Planetary Science Letters, 273(1–2): 48–57.

Chen, B., Jahn, B.M., Wilde, S.A., and Xu, B., 2000. Two contrasting Paleozoic magmatic belts in northern Inner Mongolia, China: Petrogenesis and tectonic implications. Tectonophysics, 328: 157–182.

Chen, B., Jahn, B.M., and Tian, W., 2009. Evolution of the solonker suture zone: constraints from zircon U-Pb ages, Hf isotopic ratios and whole-rock Nd-Sr isotope compositions of subduction and collision-related magmas and forearc sediments. Journal of Asian Earth Sciences, 34(3): 245–257.

Cheng, Y.H., Teng, X.J., Xin, H.T., Yang, J.Q., Shi, P., Zhang, Y., and Li, Y.F., 2012. SHRIMP zircon U-Pb dating of granites in Mahonondor area, East Ujimqin Banner, Inner Mongolia. Acta Petrologica et Mineralogica, 31(3): 323–334 (in Chinese with English abstract).

Eby, G.N., 1992. Chemical subdivision of the A-type granitoids-petrogenetic and tectonic implimplications. Geology, 20(7): 641–644.

Elhlou, S., Belousova, E., Griffin, W.L., Pearson, N.J., and O'Reilly, S.Y., 2006. Trace element and isotopic composition of GJ-red zircon standard by laser ablation. Geochimica et Cosmochimica Acta, 70 (S18): A158.

Geng, J.Z., Li, H.K., Zhang, J., Zhou, H.Y., and Li, H.M., 2011. Zircon Hf isotope analysis by means of LA-MC-ICP-MS. Geological Bulletin of China, 30(10): 1508–1513 (in Chinese with English abstract).

Griffin, W.L., Pearson, N.J., Belousova, E., Jackson, S.E., Achterbergh, E., O'Reilly, S.Y., and Shee, S.R., 2000. The Hf isotope composition of cratonic mantle: LAM-MC-ICPMS

analysis of zircon megacrysts in kimberlites. Ceochimica et Cosmochimica Acta, 64(1): 133–147.
Griffin, W.L., Wang, X., Jackson, S.E., Pearsona, N.J., O'Reilly, S.Y., Xu, X.S., and Zhou, X.M., 2002. Zircon chemistry and magma mixing, SE China: In-situ analysis of Hf isotopes, Tonglu and Pingtan igneous complexes. Lithos, 61(3–4): 237–269.
Guo, K.C., Zhang, W.L., Yang, X.P., Wang, L., Shi, D.Y., Yu, H.T., and Su, H., 2011. Origin of Early Permian A-type granite in the Wudaogou area, Heihe city. Journal of Jilin University, 41(4): 1077–1083 (in Chinese with English abstract).
Han, B.F., Zhang, C., Zhao, L., Ren, R., Zhao, X., Chen, J.F., Zhang, L., Zhou, Y.Z., and Song, B., 2010. A preliminary study of granitoids in western Inner Mongolia. Acta Petrologica et Mineralogica, 29(6): 741–749 (in Chinese with English abstract).
He, F.B., Wei, B., Xu, J.X., Sun, Y.H., and Li, R.J., 2017. Ages, origin and geological implications of the volcanic rocks in the Baoligaomiao Formation of East Ujimqin Banner, Inner Mongolia. Geology in China, 44(6): 1159–1174 (in Chinese with English abstract).
Hong, D.W., Wang, S.G., and Huang, H.Z., 1991. Preliminary study of the late Paleozoic -Triassic alkaline granite belt in northern territory of China and adiacent areas and its geodynamic significance. In: Li Z T(eds.). Contributions on granitoids and their Minerogenesis in Northern China. Beijing: Geological Publishing House, 40–48 (in Chinese).
Hong, D.W., Shi, W.G., Xi, X.L., and Ji, Z.S., 2000. Genesis of positive ε(Nd,t) granitoids in the Dahingganmts-Mongolia Orogenic Belt and growth continental crust. Earth Science Frontiers, 7(2): 441–456 (in Chinese with English abstract).
Hong, D.W., Zhang, J.S., Wang, T., Wang, S.G., and Xie, X.L., 2004. Continental crustal growth and the super continental cycle: evidence from the Central Asian Orogenic Belt. Journal of Asian Earth Sciences, 23(5): 799–813.
Irvine, T.H., and Baragar, W.R.A., 1971. A guide to the chemical classification of the common volcanic rocks. Canadian Journal of Earth Sciences, 8: 523–548.
King, P.L., White, A.J.R., Chappell, B.W., and Allen, C.M., 1997. Characterization and origin of aluminous A-type granites from the Lachlan Fold Belt, Southeasten Australia. Petrol, 38: 371–391.
Kong, L.J., Han, B.F., Zheng, B., Feng, L.X., Wang, Z.Z., and Sun, L., 2017. Geochronology, geochemistry and tectonic significances of the granites to the northeast of Erenhot, Inner Mongolia. Acta Petrologica et Mineralogica, 36(04): 433–457 (in Chinese with English abstract).
Li, S., Chung, S.L., Wilde, S.A., Wang, T., Xiao, W.J., and Guo, Q.Q., 2016. Linking magmatism with collision in an accretionary orogen. Scientific Reports 6, 25751.
Li, S., Chung, S.L., Wilde, S.A., Jahn, B.M., Xiao, W.J., Wang, T., and Guo, Q.Q., 2017. Early-Middle Triassic high Sr/Y granitoids in the southern Central Asian Orogenic Belt: Implications for ocean closure in accretionary orogens. Journal of Geophysical Research: Solid Earth, 122: 2291–2309.
Liu, J.F., 2009. Late Paleozoic magmatism and its constraints on regional tectonic evolution in Linxi-Dongwuqi area, Inner Mongolia (Ph.D. thesis). Chang chun: Jilin University, 1–157 (in Chinese with English abstract).
Liu, Y.J., Zhang, X.Z., Jin, W., Chi, X.G., Wang, C.W., Ma, Z.H., Han, G.Q., Zhao, Y.L., Wang, W.D., and Zhao, X.F., 2010. Late Paleozoic tectonics evolution in Northeast China. Geology in China, 37: 943–951 (in Chinese with English abstract).
Liu, Y.J., Li, W.M., Feng, Z.Q., Wen, Q.B., Neubauer, F., and Liang, C.Y., 2017. A review of the Paleozoic tectonics in the eastern part of Central Asian Orogenic Belt. Gondwana Research, 43: 123–147.
Liu, Y.J., Li, S.Z., Xiao, W.J., and Somerville, L., 2019. Preface: Tectonics of China. Geological Journal, 54: 631–638.
Liu, Y.S., Hu, Z.C., Gao, S., Günther, D., Xu, J., Gao, C.G., and Chen, H.H., 2008. In situ analysis of major and trace elements of anhydrous minerals by LA-ICP-MS without applying an internal standard. Chemical Geology, 257(1–2): 34–43.
Loiselle, M.C., and Wones, D.R., 1979. Characteristic and origin of anorogenic granites. Geol. Soc. Am. Abstr. Prog., 11: 468.
Ludwig, K.R., 2003. Isoplot 3.00: a geochronological toolkit for microsoft excel. California, Berkeley, Berkeley Geochronology Center, 39.
Ma, D.L., He, D.F., Di, L., Tang, J.Y., and Liu, Z., 2015. Kinematics of syn-tectonic unconformities and implications for the tectonic evolution of the Hala'alat Mountains at the northwestern margin of the Junggar Basin, Central Asian Orogenic Belt. Geoscience Frontiers, 6(2): 247–264.
Maniar, P.D., and Piccoli, P.M., 1989. Tectonic discrimination of granitoids. Geological Society of America Bulletin, 101: 635–643.
McDonough, W.F., and Sun, S.S., 1995. The composition of the earth. Chemical Geology, 120(3–4): 223–253.
Miao, L.C., Fan, W.M., Zhang, F.Q., Liu, D.Y., Jian, P., Shi, G.H., Tao, H., and Shi, Y.R., 2004. Zircon SHRIMP geochronology of the Xinkailing-Kele complex in the northwestern Lesser Xing'an Range, and its geological implications. Chinese Science Bulletin, 49(2): 201–209.
Peccerillo, A., and Taylor, S.R., 1976. Geochemistry of Eocene calc-alkaline volcanic rocks from the Kastamonu area, northern Turkey. Contrib Miner Petrol, 58: 63–81.
Pitcher, W.S., 1993. The nature and origin of granite. Academic and professional, London: Chapman and Hall, 1–464.
Qu, H., Li, C.L., Zhao, Z.H., Wang, Z., and Zhang, J.F., 2011. Zircon U-Pb ages and geochemical characteristics of the granites in Duobaoshan area, Northeast Da Hinggan Mountains. Geology in China, 2(38): 292–300 (in Chinese with English abstract).
Şengor, A.M.C., Boris, A., and Natal'in, B.A., 1996. Paleotectonics of Asia: Fragments of a synthesis. In: An, Y., and Mark, H. (eds.). The tectonic evolution of Asia. Cambridge: Cambridge University Press, 486–640.
Shao, J.A., Tang, K.D., and He, G.Q., 2014. Early Permian tectono-palaeogeographic reconstruction of Inner Mongolia, China. Acta Petrologica Sinica, 30(7): 1858–1866 (in Chinese with English abstract).
Shi, G.H., Miao, L.C., Zhang, F.Q., Jian, P., Fan, W.M., and Liu, D.Y., 2004. Emplacement age and tectonic implications of the Xilinhot A-type granite in Inner Mongolia, China. Chinese Science Bulletin, 49(7): 723–729.
Shi, Y., Yao, Y., Liu, Z.H., Liu, J., Wei, M.H., Gu, Y.C., Yang, F., Zhang, L., and Shi, S.S., 2019. Petrogeochemical characteristics, zircon SHRIMP U-Pb ages and Lu-Hf isotopic compositions of Late Carboniferous A-type granitoids, Yili area, Inner Mongolia (China). Geological Journal, 54(2): 770–790.
Stille, P., and Steiger, R.H., 1991. Hf isotope systematics in granitoids from the central and southern Alps. Contributions to Mineralogy and Petrology, 107(3): 273–278.
Sui, Z.M., Ge, W.C., Xu, X.C., and Zhang, J.H., 2009. Characteristics and geological implications of the late Paleozoic post-orogenic Shierzhan granite in the Great Xing'an Range. Acta Petrologica Sinica, 25(10): 2679–2686 (in Chinese with English abstract).
Sun, S.S., and McDonough, W.F., 1989. Chemical and isotopic systematics of oceanic basalts: Implications for mantle composition and processes. Geological Society of London Special Publications, 42: 313–345.
Sun, D.Y., Wu, F.Y., Li, H.M., and Lin, Q., 2001. Emplacement age of the postorogenic A-type granites in northwestern Lesser Xing'an Ranges, and its relationship to the eastward extension of Suolushan-Hegenshan-Zhalaite collisional suture zone. Chinese Science Bulletin, 46(5): 427–432.
Tang, J.Y., He, D.F., Li, D., and Ma, D.L., 2015. Large-scale thrusting at the northern Junggar basin since Cretaceous and its implications for the rejuvenation of the Central Asian Orogenic Belt. Geoscience Frontiers, 6(2): 227–246.
Taylor, S.R., and Mclennan, S.M., 1985. The continental crust: Its composition and evolution, an examination of the geochemical record preserved in sedimentary rocks. Journal of Geology, 94(4): 632–633.
Tong, Y., Hong, D.W., Wang, T., Shi, X.J., Zhang, J.J., and Zeng, T., 2010. Spatial and temporal distribution of granitoids

in the middle segment of the Sino-Mongolian Border and its tectonic and metallogenic implications. Acta Geoscientica Sinica, 31(3): 395–412 (in Chinese with English abstract).
Tong, Y., Jahn, B.M., Wang, T., Hong, D.W., Smith, E.I., Sun, M., Guo, J.F., Yang, Q.D., and Huang, W., 2015. Permian alkaline granites in the Erenhot-Hegenshan belt, northern Inner Mongolia, China: Model of generation, time of emplacement and regional tectonic significance. Journal of Asian Earth Sciences, 97(Part B): 320–336.
Wang, T., Jahn, B.M., Kovach, V.P., Tong, Y., Hong, D.W., and Han, B.F., 2009. Nd-Sr isotopic mapping of the Chinese Altai and implications for continental growth in the Central Asian Orogenic Belt. Lithos, 110(1–4): 359–372.
Wang, S.Q., Hu, X.J., Zhao, H.L., Xin, H.T., Yang, Z.L., Liu, W.G., and Li, H., 2017. Geochronology and geochemistry of Late Carboniferous Jinggesitai alkaline granites, Inner Mongolia: Petrogenesis and implications for tectonic evolution. Acta Geologica Sinica, 91(7): 1467–1482 (in Chinese with English abstract).
Whalen, J.B., Currie, K.L., and Chappell, B.W., 1987. A-type granites: Geochemical characteristics, discrimination and petrogenesis. Contributions to Mineralogy and Petrology, 95 (4): 407–419.
Wu, F.Y., Jahn, B.M., Wilde, S.M., and Sun, D.Y., 2000. Phanerozoic crustal growth: U-Pb and Sr-Nd isotopic evidence from the granites in northeastern China. Tectonophysics, 328(1–2): 89–113.
Wu, F.Y., Sun, D.Y., Li, H.M., Jahn, B.M., and Wilde, S.M., 2002. A-type granites in northeastern China: age and geochemical constraints on their petrogenesis. Chemical Geology, 187(1–2): 143–173.
Wu, F.Y., Li, X.H., Zheng, Y.F., and Gao, S., 2007. Lu-Hf isotopic systematics and their applications in petrology. Acta Petrologica Sinica, 23(2): 185–220 (in Chinese with English abstract).
Xia, L.Q., Xu, X.Y., Li, X.M., Ma, Z.C., and Xia, X.A., 2012. Reassessment of petrogenesis of Carboniferous—Early Permian rift-related volcanic rocks in the Chinese Tianshan and its neighboring areas. Geoscience Frontiers, 3(4): 445–471.
Xiao, W.J., Zhang, L.C., Qin, K.Z., Sun, S., and Li, J.L., 2004. Paleozoic accretionary and collisional tectonics of the eastern Tienshan(China): Implications for the continental growth of Central Asian. Journal of Science, 304(4): 370–395.
Xiao, W.J., Windley, B.F., Huang, B.C., Han, C.M., Yuan, C.K., Chen, H.L., Sun, S., and Li, J.L., 2009a. End-Permian to mid-Triassic termination of the accretionary processes of the southern Altaids: Implications for the geodynamic evolution, Phanerozoic continental growth, and metallogeny of Central Asia. International Journal of Earth Sciences, 98(6): 1189–1217.
Xiao, W.J., Kroner, A., and Windley, B.F., 2009b. Geodynamic evolution of central Asia in the Paleozoic and Mesozoic. International Journal of Earth Sciences, 98(1): 1185–1188.
Xiao, W.J., and Santosh, M., 2014. The western Central Asian Orogenic Belt: A window to accretionary orogenesis and continental growth. Gondwana Research, 25(4): 1429–1444.
Xiao, W.J., and Santosh, M., 2015. Continental reconstruction and metallogeny of the Circum-Junggar areas and termination of the southern Central Asian Orogenic Belt. Geoscience Frontiers, 6(2): 137–140.
Xin, H.T., Teng, X.J., and Cheng, Y.H., 2011. Stratigraphic subdivision and isotope geochronology study on the Baoligaomiao Formation in the East Ujimqin County, Inner Mongolia. Geological Survey and Research, 34(1): 1–9 (in Chinese with English abstract).
Xu, B., Zhao, P., Bao, Q.Z., Zhou, Y.H., Wang, Y.Y., and Luo, Z.W., 2014. Preliminary study on the pre-Mesozoic tectonic unit division of the Xing-Meng Orogenic Belt (XMOB). Acta Petrologica Sinica, 30(7): 1841–1857 (in Chinese with English abstract).
Xue, H.M., Guo, L.J., Hou, Z.Q., Tong, Y., Pan, X.F., and Zhou, X.W., 2010. SHRIMP zircon U-Pb ages of the middle Neopaleozoic unmetamorphosed magmatic rocks in the southwestern slope of the Dahinggan Mountains, Inner Mongolia. Acta Petrologica et Mineralogica, 29(6): 811–823 (in Chinese with English abstract).
Yang, D., Chen, M., Gong, Q.D., Chen, T.H., Huang, F., Wu, H., and Li, H.L., 2017. Geochemical characteristics, zircon U-Pb ages of the late Carboniferous granite in Baiyintuga area, Abaga Banner, Inner Mongolia and their geological significance. Geological Review, 63(05): 1209–1225 (in Chinese with English abstract).
Zhang, J., Ge, W.C., Li, B.Y., Gao, Y., and Hang, Y.L., 2011. Zircon U-Pb ages and Hf isotopes of late Paleozoic granites in Taerqi area, Inner Mongolia. Global Geology, 30(04): 521–531 (in Chinese with English abstract).
Zhang, Q., Ran, H., and Li, C.D., 2012. A-type granite: what is the essence? Acta Petrologica et Mineralogica, 31(4): 621–626 (in Chinese with English abstract).
Zhang, X.H., Yuan, L.L., Xue, F.H., Yan, X., and Mao, Q., 2016. Early Permian A-type granites from central Inner Mongolia, North China: Magmatic tracer of post-collisional tectonics and oceanic crustal recycling. Gondwana Research, 28(1): 311–327.
Zhang, X.Z., Yang, B.J., Wu, F.Y., and Liu, G.X., 2006. The lithosphere structure in the Hingmong-Jihei (Hinggan-Mongolia-Jilin-Heilongjiang) region, northeastern China. Geology in China, 33(4): 816–823 (in Chinese with English abstract).
Zhang, Y.Q., Xu, L.Q., Kang, X.L., and Bao, Y.W.L.J., 2009. Age dating of alkali granite in Jingesitai area of Dong Ujimqin banner, Inner Mongolia, and its significance. Geology in China, 36(5): 988–995 (in Chinese with English abstract).
Zhang, Z.J., Chen, Y.J., Chen, H.Y., Bao, J.X., and Liu, Y.L., 2003. The petrochemical characteristics of the Hercynian granitoids in Tianshan and its geodynamic implication. Journal of Mineralogy and Petrology, 22(2): 13–21.
Zhao, Y.D., Zhao, J., Wang, K.L., Che, J.Y., Da, T., Xu, F.M., and Li, S.C., 2013. Characteristics of the late Carboniferous post-orogenic Dayinhe intrusion in the northwest of the Xiao Hinggan Mountains and their geological implications. Acta Petrologica et Mineralogica, 26(08): 2452–2464 (in Chinese with English abstract).
Zhao, Z., Chi, X.G., Pan, S.Y., Liu, J.F., Sun, W., and Hu, Z.C., 2010. Zircon U-Pb LA-ICP-MS dating of Carboniferous volcanics and its geological significance in the northwestern Lesser Xing'an Range. Acta Petrologica Sinica, 26(8): 2452–2464 (in Chinese with English abstract).
Zhou, J.B., Han, J., Zhao, G.C., Zhang, X.Z., Cao, J.L., Wang, B., and Sheng, H.P., 2015. The emplacement time of the Hegenshan ophiolite: Constraints from the unconformably overlying Paleozoic strata. Tectonophysics, 662: 398–415.
Zhou, Y.Z., 2011. Progress made in A-type granite study and discussion on some issues. Geology of Anhui, 21(3): 169–175 (in Chinese with English abstract).

About the first author



ZHANG Li, male, born in 1987 in Qitaihe City, Heilongjiang Province, master, graduated from College of Earth Sciences, Jilin University, Changchun, engineer of Shenyang Institute of Geology and Mineral Resources, China Geological Survey, Shenyang. He is now interested in study on the evolution of the Paleo-Asian Tectonic Domain. E-mail: zl_jlu2012 @163.com, Phone: 024–81847035.

About the corresponding author



LIU Yongjiang, male, born in 1964 in Mudanjiang City, Heilongjiang Province, Doctor, professor of Key Lab of Submarine Geoscience and Prospecting Techniques, MOE, Institute for Advanced Ocean Study, College of Marine Geosciences, Ocean University of China, Qingdao. He is now interested in study on geotectology and tectonic chronology. E-mail: liuyongjiang@ouc.edu.cn. Phone: 0532–66785928.